

# Crafting the dynamical structure of synchronization by harnessing bosonic multilevel cavity QED

**Journal Article****Author(s):**

Valencia-Tortora, Riccardo J.; Kelly, Shane P.; [Donner, Tobias Ulrik](#) ; Morigi, Giovanna; Fazio, Rosario; Marino, Jamir

**Publication date:**

2023

**Permanent link:**

<https://doi.org/https://doi.org/10.3929/ethz-b-000612856>

**Rights / license:**

[Creative Commons Attribution 4.0 International](#)

**Originally published in:**

Physical Review Research 5(2), <https://doi.org/10.1103/physrevresearch.5.023112>

**Funding acknowledgement:**

- Cavity-assisted pattern recognition ()

**Crafting the dynamical structure of synchronization by harnessing bosonic multilevel cavity QED**Riccardo J. Valencia-Tortora <sup>1,\*</sup>, Shane P. Kelly,<sup>1</sup> Tobias Donner,<sup>2</sup> Giovanna Morigi,<sup>3</sup> Rosario Fazio,<sup>4,5</sup> and Jamir Marino<sup>1</sup><sup>1</sup>*Institut für Physik, Johannes Gutenberg-Universität Mainz, D-55099 Mainz, Germany*<sup>2</sup>*Institute for Quantum Electronics, Eidgenössische Technische Hochschule Zürich, Otto-Stern-Weg 1, CH-8093 Zurich, Switzerland*<sup>3</sup>*Theoretical Physics, Department of Physics, Saarland University, 66123 Saarbrücken, Germany*<sup>4</sup>*The Abdus Salam International Center for Theoretical Physics (ICTP), I-34151 Trieste, Italy*<sup>5</sup>*Dipartimento di Fisica, Università di Napoli Federico II, Monte S. Angelo, I-80126 Napoli, Italy*

(Received 7 December 2022; accepted 25 April 2023; published 19 May 2023)

Many-body cavity QED experiments are established platforms to tailor and control the collective responses of ensembles of atoms, interacting through one or more common photonic modes. The rich diversity of dynamical phases they can host calls for a unified framework. Here we commence this program by showing that a cavity QED simulator assembled from  $N$ -level bosonic atoms can reproduce and extend the possible dynamical responses of collective observables occurring after a quench. Specifically, by initializing the atoms in classical or quantum states, or by leveraging intralevel quantum correlations, we craft on demand the entire synchronization/desynchronization dynamical crossover of an exchange model for  $SU(N)$  spins. We quantitatively predict the onset of different dynamical responses by combining the Liouville-Arnold theorem on classical integrability with an ansatz for reducing the collective evolution to an effective few-body dynamics. Among them, we discover a synchronized chaotic phase induced by quantum correlations and associated to a first-order nonequilibrium transition in the Lyapunov exponent of collective atomic dynamics. Our outreach includes extensions to other spin-exchange quantum simulators and a universal conjecture for the dynamical reduction of nonintegrable all-to-all interacting systems.

DOI: [10.1103/PhysRevResearch.5.023112](https://doi.org/10.1103/PhysRevResearch.5.023112)**I. INTRODUCTION**

Tailoring light-matter interactions is at the root of numerous technological and experimental applications in quantum optics, and it has generated a persistent drive for better control of atoms and photons since the advent of modern molecular and atomic physics. For instance, the pursuit to create precision clocks and sensors has led to the development of cavity QED systems in which a cold gas couples to few or several electromagnetic modes in an optical cavity [1–6]. Such systems can be brought out of equilibrium to generate reproducible many-body dynamics which show complex behavior including self-organization [4,7–15] and dynamical phase transitions [1,6,12,16–20], quantum squeezed and non-Gaussian entangled states [21–27], time crystals [28–31], and glassy dynamics [10,13,32,33]. This rich phenomenology comes from a high degree of tunability in such systems, allowing control over local external fields, detunings between cavity mode and applied drive fields, the ability to couple multiple atomic levels to the cavity field [5,10,34–39], and,

more recently, the realization of programmable geometries for light-matter interactions [40–42].

Recently, the theoretical and experimental investigation of multilevel cavity systems has gathered increasing attention. Current progress includes dissipative state preparation of entangled dark states [43–45], multicriticality in generalized Dicke-type models [46,47], incommensurate time crystalline phases [35,48,49], correlated pair creations and phase-coherence protection via spin-exchange interactions [37,50,51], spin squeezing, and atomic clock precision enhancement [52–54]. Yet, the quenched dynamics in multilevel cavity systems is widely unexplored and the few individual results lack an organizing principle.

In this paper, we propose a unifying framework for the dynamics after a quench of all-to-all connected multilevel systems. We show that the flexible control endowed by bosonic multilevel atoms is sufficient to reproduce established dynamical phases and beyond. We explain how the dynamical response can be crafted into these dynamical phases by introducing a reduction of dynamics to a few-body effective classical evolution, valid regardless of the underlying integrability of the model. Of particular note, we demonstrate how quantum correlations in the initial state can drive a transition between a regular and chaotic synchronized phases.

Our analysis extends the established phenomenology of the two-level Tavis-Cummings model with local inhomogeneous fields. This two-level model is integrable [55], and allows for the emergent collective many-body dynamics to be exactly described through an effective few-body Hamiltonian [56–66].

\*rvalenci@uni-mainz.de

Published by the American Physical Society under the terms of the [Creative Commons Attribution 4.0 International](https://creativecommons.org/licenses/by/4.0/) license. Further distribution of this work must maintain attribution to the author(s) and the published article's title, journal citation, and DOI.

In particular, the few-body model yields predictions for the dynamical responses of collective observables  $S(t)$ , such as the collective spin raising operator, given by the macroscopic sum of several individual constituents [56,59,60,63–67]. The resulting dynamical phases are best presented in terms of the possible synchronization between the local atomic degree of freedoms (DOFs) (spins-1/2) which evolve with a frequency set by the competition of their local field and collective photon-mediated interactions. In the desynchronized phase, which we call phase I as shorthand, all the spins evolve independently as a result of dominant classical dephasing processes imprinted by the local inhomogeneous fields, thus  $S(t)$  relaxes to zero. In the synchronized phase, collective interactions lock the phase precession and we can distinguish three different scenarios in which  $S(t)$  either relaxes to a stationary value (phase II), up to a phase of a Goldstone mode [56] associated to a global U(1) symmetry, or its magnitude enters self-generated oscillatory dynamics, corresponding to a Higgs mode [56], either periodic (phase III) or aperiodic (phase IV). While phases I and II describe relaxation to a steady state up to an irrelevant global phase, phases III and IV are instead examples of a self-generated oscillating synchronization phenomenon without an external driving force [68–71].

### A. Summary of results

In this paper, we investigate dynamics beyond two-level approximations by considering  $\mathcal{N}_a$  bosonic atoms, each hosting  $N$  levels which realize SU( $N$ ) spins. The additional structure due to the bosonic statistics allows us to naturally consider both classical and quantum initial states (cf. Sec. II C). Using this flexibility in the initial state, and also the tunability of Hamiltonian parameters, we show how to craft not only the dynamical responses present in the two-level integrable setup (from phase I up to phase IV), but also how to access a chaotic dynamical response. This chaotic response, which we refer to as phase IV\*, again has all atoms synchronized but with the dynamics of the average atomic coherences characterized by exponential sensitivity to initial conditions. The self-generated chaotic phase IV\* emerges from the interplay of initial quantum correlations and the collective interactions mediated by the cavity field. It is therefore qualitatively different from chaos induced by other mechanisms as due to additional local interactions [72] or external pump [30,73–76].

To show how to craft and control these dynamical responses, we introduce a generalization of the reduction hypothesis used for two-level systems. Specifically, we propose that the different dynamical phases (phase I up to phase IV\*) all correspond to a different effective few-body Hamiltonian that depends on the global symmetries of the many-body system, degree of inhomogeneity,  $W$ , number of atomic levels  $N$ , and degree of quantum correlations in the initial state, quantified by a parameter  $p$  (cf. Sec. IV B). Then, by considering an appropriate classical limit arising in the limit of large system size (cf. Sec. II B), we apply the Liouville-Arnold theorem to the effective Hamiltonian to identify a correspondence between the dynamical phases and the effective Hamiltonians. Using physical arguments for the

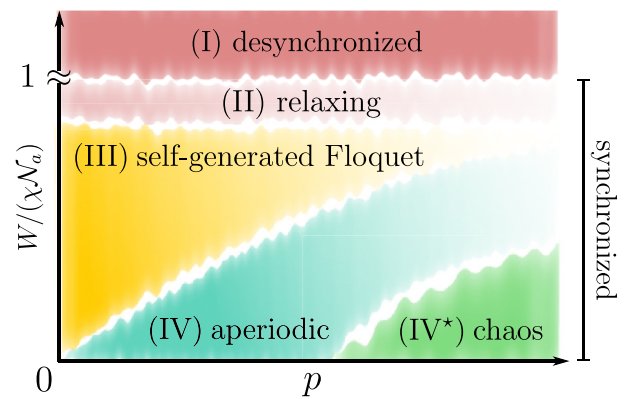


FIG. 1. Cartoon of the possible dynamical responses of intralevel phase coherence in a photon-mediated spin-exchange model between SU(3) spins as a function of the degree of inhomogeneity of the local fields  $W$  and of quantum correlations in the initial state parameterized by  $p$ . At  $p = 0$ , each site is initialized in the same bosonic coherent state. For  $p > 0$ , there are finite quantum correlations in the system. The parameter  $p$  tunes from bosonic coherent states ( $p = 0$ ) to a multimode Schrödinger cat state ( $p > 0$ ) initialized on each site. The susceptibility of the dynamical response to quantum correlations is strictly linked to having SU( $N$ ) spins with  $N > 2$ , and thus cannot be achieved considering two-level systems. Up to inhomogeneity  $W/(\chi\mathcal{N}_a) \approx 1$ , the system is in the synchronized phase. At larger inhomogeneities, the system enters in the desynchronized phase and all phase coherence is washed (phase I). In the synchronized phase, phase coherence relaxes asymptotically to a nonzero value up to a phase associated to a global U(1) symmetry (phase II), or its magnitude enters a self-generated oscillatory dynamics, either periodic (phase III) or aperiodic (phase IV), as well as potentially chaotic (phase IV\*). In this last case, dynamics are exponentially sensitive to changes in initial conditions.

nature of the effective Hamiltonian, we then predict how to tune between different dynamical responses. The result is an intuitive control over the rich dynamical response possible in multilevel cavity QED. See Fig. 1 for a cartoon of the different dynamical responses for  $N = 3$  level atoms, using as a proxy the synchronized (or desynchronized) evolution of the magnitude of the average intralevel coherences in the ensemble. We conclude by discussing the potential universality of the reduction hypothesis. In particular, we conjecture it applies not only for state-of-the-art cavity QED experiments (cf. Sec. VI), but could find potential applications in other fields. Following Refs. [77,78], where cavity QED platforms are proposed to model the dynamics of  $s$ -wave and  $(p + ip)$ -wave BCS superconductors, our results could find potential applications to lattice systems with local SU( $N$ ) interactions, such as SU( $N$ ) Hubbard models [79–82]. Another possible outreach of our results could consist of noticing that the  $N$  levels of the atoms could be used as a synthetic dimension, with the geometry fixed by the photon-mediated processes, as, for instance, in a synthetic ladder system [83,84]. Furthermore, since we consider bosonic systems, our results could potentially find applications in spinor Bose-Einstein condensates [85,86] or in molecules embedded in a cavity, where bosons could be identified as their vibrational modes [87,88].

## B. Organization of the paper

The paper is organized as follows. In Sec. II, we introduce the model and initial states we investigate and discuss the cumulant expansion we use to capture quench dynamics. In Sec. III, we present the dynamical reduction hypothesis and discuss the different classes of effective dynamics that can result from it. In Sec. IV, we show that in the homogeneous limit our hypothesis is exact and demonstrate how local quantum correlations in SU(3) atoms can induce a chaotic dynamical phase with finite Lyapunov exponent. In Sec. V, we show that the dynamical responses observed in the homogeneous limit are robust against moderate inhomogeneity in the local fields, and we provide numerical evidence that an effective few-body Hamiltonian is able to capture the dynamical periodic response of collective observables in the three-level case. We conclude this section with a discussion on the impact of inhomogeneity in the dynamical responses of the system. In Sec. VI, we propose an experimental implementation potentially accessible in state-of-the-art cavity QED systems.

## II. PRELIMINARIES

### A. The model

We consider a system of  $\mathcal{N}_a$  bosonic atoms interacting via a single photonic mode of a cavity. The atoms are cooled to the motional ground state and evenly distributed among  $L$  different atomic ensembles labeled by a site index  $j$ . Within each site (ensemble), the atoms are indistinguishable and can occupy  $N$  different atomic levels with energies that are site and level dependent. We consider the atoms sufficiently far apart for interatomic interactions to be negligible. The photon-matter interaction mediates atom number conserving processes where the absorption and/or the emission of a cavity photon results in an atom transitioning from level  $n$  to levels  $n \pm 1$  within the same site, with a rate generally dependent on the specific level  $n$ . The associated many-body light-matter Hamiltonian reads

$$\begin{aligned} \hat{H} = & \omega_0 \hat{a}^\dagger \hat{a} + \sum_{j=1}^L \sum_{n=1}^N h_n^{(j)} \hat{b}_{n,j}^\dagger \hat{b}_{n,j} \\ & + \sum_{j=1}^L \sum_{n=1}^{N-1} [g_n (\hat{b}_{n+1,j}^\dagger \hat{b}_{n,j} \hat{a} + \text{H.c.}) \\ & + \lambda_n (\hat{b}_{n+1,j}^\dagger \hat{b}_{n,j} \hat{a}^\dagger + \text{H.c.})], \end{aligned} \quad (1)$$

where  $\hat{a}^{(\dagger)}$  is the bosonic annihilation (creation) operator of the cavity photon;  $\hat{b}_{n,j}^{(\dagger)}$  is the bosonic annihilation (creation) operator on site  $j \in [1, L]$  and level  $n \in [1, N]$ , with energy splitting  $h_n^{(j)}$ ;  $g_n$  and  $\lambda_n$  are the single-particle photon-matter couplings which controls rotating and corotating processes, respectively. Tuning  $g_n$  and  $\lambda_n$  enables us to pass from a generalized multilevel Dicke model, when  $g_n, \lambda_n \neq 0$ , to the multilevel Tavis-Cummings model, when  $\lambda_n = 0$ . In our paper, we consider dynamics on timescales where dissipative processes are subdominant compared to coherent evolution (cf. Sec. VII A).

When the cavity is far detuned from the atomic transitions, the photon does not actively participate in dynamics of Eq. (1)

but instead mediates virtual atom-atom interactions [89]. This occurs in the limit  $\omega_0 \gg \max\{h_n^{(j)}, g_n \sqrt{\mathcal{N}_a}, \lambda_n \sqrt{\mathcal{N}_a}\}$ , where the factor  $\sqrt{\mathcal{N}_a}$  comes from the cooperative enhancement given by the  $\mathcal{N}_a$  atoms [90,91]. The mediated interaction results in an effective atoms-only Hamiltonian of the form

$$\begin{aligned} \hat{H} = & \sum_{j=1}^L \sum_{n=1}^N h_n^{(j)} \hat{\Sigma}_{n,n}^{(j)} - \sum_{m,n=1}^{N-1} [\chi_{n,m} \hat{\Sigma}_{n+1,n} \hat{\Sigma}_{m,m+1} \\ & + \zeta_{n,m} \hat{\Sigma}_{n,n+1} \hat{\Sigma}_{m+1,m} + \nu_{n,m} \hat{\Sigma}_{n+1,n} \hat{\Sigma}_{m+1,m} \\ & + \nu_{m,n} \hat{\Sigma}_{n,n+1} \hat{\Sigma}_{m,m+1}], \end{aligned} \quad (2)$$

where  $\chi_{n,m} \equiv g_n g_m / \omega_0$ ;  $\zeta_{n,m} \equiv \lambda_n \lambda_m / \omega_0$ ;  $\nu_{n,m} \equiv \lambda_n g_m / \omega_0$ . For convenience, we have written the Hamiltonian in Eq. (2) as a function of the operators

$$\hat{\Sigma}_{n,m}^{(j)} = \hat{b}_{n,j}^\dagger \hat{b}_{m,j}, \quad (3)$$

$$\hat{\Sigma}_{n,m} = \sum_{j=1}^L \hat{\Sigma}_{n,m}^{(j)}. \quad (4)$$

The operators  $\{\hat{\Sigma}_{n,m}^{(j)}\}$  are generators of the SU( $N$ ) group [92,93] and they obey the commutation relations  $[\hat{\Sigma}_{n,m}^{(i)}, \hat{\Sigma}_{k,l}^{(j)}] = \delta_{i,j} (\hat{\Sigma}_{n,l}^{(i)} \delta_{m,k} - \hat{\Sigma}_{k,m}^{(j)} \delta_{n,l})$ , and  $(\hat{\Sigma}_{n,m}^{(j)})^\dagger = \hat{\Sigma}_{m,n}^{(j)}$ .

The regime we are mostly interested in is  $\nu_{n,m} = \zeta_{n,m} = 0$ , which translates to  $\lambda_n = 0$ . In this limit, the Hamiltonian in Eq. (2) turns into a spin-exchange interaction Hamiltonian between SU( $N$ ) spins with rates  $\{\chi_{n,m}\}$  and inhomogeneous fields,  $h_n^{(j)}$ . In the following, we set the collective spin-exchange rate  $\chi \mathcal{N}_a = \mathcal{N}_a \sum_{n=1}^{N-1} \chi_{n,n}$  as our energy scale, such that the timescales of our results are independent of the number of atoms  $\mathcal{N}_a$  in the system. An implementation of the spin exchange model in Eq. (2) is offered in Sec. VI.

Below, we consider both situations when the energies of the atomic levels are homogenous and when they are inhomogenous. In the latter situation, we expect our results to hold for various forms of inhomogenities, but we will, in particular, focus on the situations when the atomic levels on each site are in an evenly spaced ladder configuration with spacing  $\Delta h_j \equiv (h_{n+1}^{(j)} - h_n^{(j)})$  sampled from a box distribution with zero average and width  $W$ . In this case, the Hamiltonian is spatially inhomogeneous for  $W = 0$  and spatially inhomogeneous for  $W > 0$ . At  $W = 0$ , we can make precise predictions of the dynamical responses as a function of the features of the initial state and multilevel structure. Then, we show numerically their robustness against many-body dynamics due to inhomogenities ( $W > 0$ ), in a fashion reminiscent of a synchronization phenomenon.

Given an evenly spaced ladder configuration within each site, the Hamiltonians in Eqs. (1) and (2) can, for certain values of the couplings  $g_n$  and  $\lambda_n$ , be written in terms of the generators of a subgroup of SU( $N$ ). For instance, in the  $N = 3$  level case, if  $g_n = g$  and  $\lambda_n = \lambda$ , the Hamiltonian can be written as a function of the generators of a SU(2) subgroup of SU(3). Specifically, only the SU(2) operators  $\hat{S}_j^- = \sqrt{2}(\hat{\Sigma}_{1,2}^{(j)} + \hat{\Sigma}_{2,3}^{(j)})$ ,  $\hat{S}_j^+ = (\hat{S}_j^-)^\dagger$ , and  $\hat{S}_j^z = (\hat{\Sigma}_{3,3}^{(j)} - \hat{\Sigma}_{1,1}^{(j)})$  are required to represent the Hamiltonian and, as a consequence, the dynamics can be more simply described by the dynamics of these SU(2) spins. For instance, we recover the

spin-1 Dicke model for  $\lambda = g$  and the spin-1 Tavis-Cummings model for  $\lambda = 0$  in Eq. (1). Since we aim to explore the impact of genuine interactions between  $SU(N)$  spins, we fix  $g_n$  and  $\lambda_n$  such that the dynamics cannot be restricted to a subgroup of  $SU(N)$  if not otherwise specified. An important exception is the three-level case, where the system can enter in a chaotic phase upon passing from interactions between  $SU(2)$  to  $SU(3)$  spins (see Sec. IV B). We highlight that while the interactions considered lead to nontrivial effects in the  $SU(N)$  DOFs, they are not  $SU(N)$  symmetric.

## B. Mean-field limit

Given a generic interacting Hamiltonian, the dynamics of any  $n$ -point correlation function depends on higher order correlation functions—a structure known as the BBGKY hierarchy [94]. In fully connected systems, as in our case, the hierarchy can be efficiently truncated starting from separable states or, in other words, from a Gutzwiller-type ansatz [95]

$$|\Psi\rangle = \otimes_{j=1}^L |\psi_j\rangle \otimes |\alpha\rangle, \quad (5)$$

where  $|\psi_j\rangle$  is a generic state on the  $j$ th atom and  $|\alpha\rangle$  is a bosonic coherent state describing the cavity field. Given  $|\Psi\rangle$  in Eq. (5), the hierarchy can be truncated as  $\langle \hat{\Sigma}_{n,m}^{(j)} \hat{a} \rangle = \langle \hat{\Sigma}_{n,m}^{(j)} \rangle \langle \hat{a} \rangle$  and  $\langle \hat{\Sigma}_{n,m}^{(j)} \hat{\Sigma}_{r,s} \rangle = \langle \hat{\Sigma}_{n,m}^{(j)} \rangle \langle \hat{\Sigma}_{r,s} \rangle$  up to  $1/L$  corrections [55,90,96–98]. Here and from now on, we assume all expectation values are taken with respect to the state  $|\Psi\rangle$ , i.e.,  $\langle \hat{o}(t) \rangle \equiv \langle \Psi | \hat{o}(t) | \Psi \rangle$ . In the limit  $L \rightarrow \infty$ , no additional quantum correlations build up in time, hence the equation of motions of one-point and two-point correlation functions are exactly closed at all times and the state  $|\Psi\rangle$  remains an exact ansatz of the many-body state.

Combining the large  $L$  limit and the nature of the interaction in the Hamiltonian, the dynamics of  $\langle \hat{\Sigma}^{(j)} \rangle$  and  $\langle \hat{a} \rangle$  can be accordingly obtained in the mean-field limit of the Hamiltonians in Eqs. (1) and (2). This is achieved replacing the operators  $\hat{\Sigma}_{n,m}^{(j)}$  and  $\hat{a}^{(\dagger)}$  by classical  $SU(N)$  spins and photon amplitude given by

$$\Sigma_{n,m}^{(j)} = \langle \hat{\Sigma}_{n,m}^{(j)} \rangle / (\mathcal{N}_a/L), \quad a = \langle \hat{a} \rangle / \sqrt{\mathcal{N}_a}, \quad (6)$$

with  $\mathcal{N}_a/L$  the average number of bosonic excitations per site and by substituting the commutators with Poisson brackets. The same dynamics can be obtained starting from the Heisenberg equation of motions and then taking the expectation value on the state  $|\Psi\rangle$  in Eq. (5) [93], truncating the hierarchy as discussed above.

The hierarchy can be further truncated at first order in the bosonic operators if the one-body reduced density matrix  $\Sigma^{(j)}$ , with matrix elements  $\Sigma_{n,m}^{(j)}$ , is pure ( $\text{Tr}[(\Sigma^{(j)})^2] = 1$ ), namely, there are no quantum correlations on a given site  $j$ . For instance, if the state  $|\psi_j\rangle$  in Eq. (5) is a bosonic coherent state on each level of site  $j$ , the matrix  $\Sigma^{(j)}$  is pure and straightforwardly factorized as  $\Sigma_{n,m}^{(j)} = \langle \hat{b}_{n,j}^\dagger \rangle \langle \hat{b}_{m,j} \rangle$ . The truncation at first order in the bosonic operators well approximates the full dynamics up to corrections which are suppressed [99] in both the number of sites  $L$  and the occupation on each site  $\mathcal{N}_a/L$ . Therefore, in the limit  $\mathcal{N}_a \rightarrow \infty$ , the hierarchy is exactly truncated at first order in the bosonic amplitudes  $\langle \hat{b}_{n,j}^{(\dagger)} \rangle$  and  $\langle \hat{a} \rangle$  at all times. In this limit, their dynamics can be

equivalently obtained in the classical limit of the Hamiltonians in Eqs. (1) and (2) by replacing the bosonic operators  $\hat{b}_{n,j}^{(\dagger)}$  and  $\hat{a}$  by the classical fields

$$b_{n,j} = \langle \hat{b}_{n,j} \rangle / \sqrt{\mathcal{N}_a/L}, \quad a = \langle \hat{a} \rangle / \sqrt{\mathcal{N}_a}, \quad (7)$$

and replacing commutators with Poisson brackets.

In the following sections, we will investigate the collective dynamical response of multilevel atoms in both mean-field limits. We will show that the dynamical response could be highly susceptible to quantum correlations in the multilevel atom case, while it is insensitive in the two-level case.

## C. Initial states

In this paper, we derive general results which can be applied to any state of the form given in Eq. (5). As discussed in Sec. II B, we distinguish two different classical limits, arising in the large  $L$  limit, corresponding to the one-body reduced density matrix  $\Sigma^{(j)}$  on site  $j$  being pure or mixed, respectively. For the sake of concreteness, we now present a few states corresponding to the two cases discussed above. The first two states are a bosonic coherent state and a  $SU(N)$  spin-coherent state, both having no quantum correlations and a one-body reduced density matrix that is pure. While the other is a multimode Schrödinger cat state, whose one-body reduced density matrix on a given site is mixed, reflecting the presence of quantum correlations.

### 1. Coherent states

The most general bosonic coherent state  $|\psi_j\rangle$  on a given site  $j$  reads

$$\begin{aligned} |\psi_j\rangle &= \exp(\boldsymbol{\gamma}_j \cdot \hat{\mathbf{b}}_j^\dagger - \text{H.c.}) |0\rangle \equiv |\tilde{\gamma}_j\rangle, \\ \boldsymbol{\gamma}_j &\equiv (\gamma_{1,j}, \gamma_{2,j}, \dots, \gamma_{N,j}), \\ \hat{\mathbf{b}}_j^\dagger &\equiv (\hat{b}_{1,j}^\dagger, \hat{b}_{2,j}^\dagger, \dots, \hat{b}_{N,j}^\dagger), \end{aligned} \quad (8)$$

with  $\gamma_{n,j} \in \mathbb{C}$  the amplitude of the bosonic coherent state on the  $n$ th level and site  $j$ , so the average number of particles per site is  $\sum_{n=1}^N |\gamma_{n,j}|^2 = \mathcal{N}_a/L$ . We highlight that the state in Eqs. (8) does not have an exact number of particles. Nonetheless, since the fluctuations of the number of particles are subleading with respect to the mean in the limit we consider ( $\mathcal{N}_a/L \rightarrow \infty$ ), the mean-field treatment is unaffected. Such a state has a pure one-body reduced density matrix, and will have an evolution captured by a mean-field limit characterized by the classical variables  $b_{n,j}$  and  $a$ .

### 2. $SU(N)$ spin-coherent states

The second example of state with pure one-body reduced density matrix is given by the superposition:  $|\psi_j\rangle = \sum_{n=1}^N \gamma_{n,j} \hat{b}_{n,j}^\dagger |0\rangle$ , which has one excitation per site. Once again, in this case, the mean-field limit applies. Furthermore, the choice to truncate to one particle per site is insensitive of particles' statistics: either a fermion or boson could be the single particle occupying the site, as we further elaborate in the concluding section, Sec. VII B. Such a state is the single-particle limit of the more general  $\mathcal{N}_a/L$  particle  $SU(N)$

spin-coherent state [92] defined by

$$|\psi_j\rangle = \frac{1}{\sqrt{(\mathcal{N}_a/L)!}} \left( \sum_{n=1}^N \gamma_{n,j} \hat{b}_{n,j}^\dagger \right)^{\mathcal{N}_a/L} |0\rangle, \quad (9)$$

which again has a pure one-body reduced density matrix reflecting a lack of quantum correlations. Thus, the dynamics of the classical variables  $b_{n,j}$  and  $a$  perfectly describe the dynamics of both the bosonic and  $SU(N)$  spin coherent states in the limit of a large number of bosons  $\mathcal{N}_a$ . Below we will present numerical results simulating these classical dynamics; they can be interpreted as describing the evolution of either of these two states. For the sake of simplicity, we will explicitly refer to these states as coherent states.

### 3. Schrödinger cat states

To consider a state in which the full two-point correlations of the bosons,  $\Sigma_{n,m}^{(j)}$ , must be considered, we add quantum correlations on site  $j$ . This ensures that the one-body reduced density matrix is not pure and cannot be written in the mean-field approximation,  $\Sigma_{n,m}^{(j)} \neq b_{n,j}^* b_{m,j}$ . As an example, we consider a state where each site is initialized in a multimode Schrödinger cat state [100,101], which are the multimode generalizations of entangled coherent states [102–104], given by the superposition of two bosonic coherent states  $|\tilde{\gamma}^{(m)}\rangle$  with average occupation  $\mathcal{N}_a/L$ , defined in Eq. (8), with  $m = \{1, 2\}$

$$|\psi_j\rangle = \frac{1}{\mathcal{D}} (|\tilde{\gamma}_j^{(1)}\rangle + |\tilde{\gamma}_j^{(2)}\rangle). \quad (10)$$

Here  $\mathcal{D}$  is a normalization constant. If  $|\langle \tilde{\gamma}_j^{(1)} | \tilde{\gamma}_j^{(2)} \rangle| = 1$ , the state in Eq. (10) reduces to the one in Eqs. (8). Instead, if  $|\langle \tilde{\gamma}_j^{(1)} | \tilde{\gamma}_j^{(2)} \rangle| < 1$ , the one-body reduced density matrix is mixed, reflecting the presence of quantum correlations on site  $j$  ( $\langle \hat{b}_{n,j}^\dagger \hat{b}_{m,j} \rangle_c \equiv \langle \hat{b}_{n,j}^\dagger \hat{b}_{m,j} \rangle - \langle \hat{b}_{n,j}^\dagger \rangle \langle \hat{b}_{m,j} \rangle \neq 0$ ). We anticipate that the collective dynamical response could be highly susceptible to quantum correlations in the multilevel atom case, while they do not play a role in the two-level case. As an instance, we discover the onset of chaos as  $|\langle \hat{b}_{n,j}^\dagger \hat{b}_{m,j} \rangle_c|$  increases in the  $N = 3$  levels case (cf. Sec. IV B). We highlight that quantum features of the state can only enter in initial conditions since dynamics are incapable of building quantum correlations in the mean-field limit (cf. Sec. II B).

## III. CLASSIFICATION OF DYNAMICAL RESPONSES

The main purpose of this paper is to investigate and classify the dynamical response of collective observables in multilevel cavity QED systems in the long-time limit. Specifically, we investigate the dynamics of the magnitude of the intralevel average coherences, defined as  $|\sum_{j=1}^L \Sigma_{n,m}^{(j)}|/L$  (for  $n \neq m$ ). To this end, we formulate the dynamical reduction hypothesis, which generalizes a similar procedure used for the integrable  $SU(2)$  limits of Eqs. (1) and (2). The hypothesis conjectures that the dynamics of collective observables can be captured by the Hamiltonian dynamics of a few effective collective DOFs. In the integrable case, the effective Hamiltonian has been used to quantitatively predict the dynamical responses observed, which include relaxation and persistent oscillations either periodic or aperiodic [56–66,105]. Despite lack of integrability,

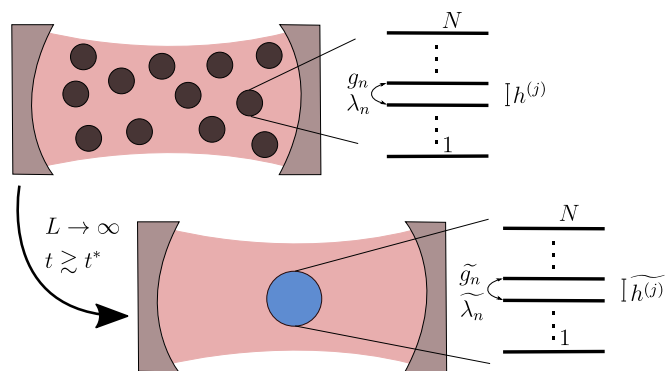


FIG. 2. Sketch of  $\mathcal{N}_a$  atoms, each one hosting  $N$  levels (panels on the side), distributed over  $L$  sites (black dots), interacting via a common cavity field (red area). In the cartoon below, we show the effective  $X$ -body system towards the original many-body system is attracted in the long time  $t \gtrsim t^*$ . We show a single-body effective model ( $X = 1$ ), since it is the one explicitly considered throughout our paper. We also show the internal structure of the single site both in the original many-body system and in the effective few-body description.

we still obtain in our case not simply relaxation but also the persistent oscillatory responses present in the integrable case, together with the possibility to develop chaos (see Fig. 3 for example) [105–107]. Due to the generic nonintegrable nature of multilevel systems, an exact procedure for extracting the effective model is not available (see Ref. [51], where the authors have attempted to extend the technique of the  $SU(2)$  case to a  $SU(N)$ -symmetric interacting spin system).

Here, we conjecture that, if an effective model exists, it is solely determined by the symmetries of the microscopic many-body problem and the relevant effective DOFs. Once the effective Hamiltonian is fixed, we show that the classification of dynamical responses follows from the combination of (1) the Liouville-Arnold theorem [108], which sets the criteria to distinguish a regular from an irregular (likely chaotic) regime, and (2) of the number of symmetries under which a given observable of interest is not invariant. Analogously to the integrable case mentioned above, we offer a classification of dynamical responses richer than the mere distinction between desynchronization and synchronization.

### A. Dynamical reduction hypothesis

In Sec. II B, we argued that, in the  $L \rightarrow \infty$  limit and for an initial state of the form given in Eq. (5), the dynamics of the cavity field and multilevel atoms are described by the equations of motion generated from a classical Hamiltonian composed of an extensive number (in the size  $L$ ) of classical  $SU(N)$  spins. The dynamical reduction hypothesis conjectures that the dynamics of collective observables are effectively described by a classical Hamiltonian composed of a finite number,  $X$ , of effective  $SU(N)$  systems (cf. Fig. 2) or, in other words, the emergent collective dynamics can be effectively captured by a few-body macroscopic system. Specifically, we conjecture that a fully connected many-body system with  $L$  sites, each with local DOFs  $s_j = \{s_{j,1}, s_{j,2}, \dots\}$ , and classical Hamiltonian  $H(\{s_j\}_{j=1}^L)$  will, after a sufficiently long time

$t \gtrsim t^*$  and in the thermodynamic limit  $L \rightarrow \infty$ , possess an  $X$ -site effective model describing the collective dynamics. The hypothesis supposes that the effective model will have  $X$  finite, even when  $L \rightarrow \infty$ , and that the effective local DOFs  $\{\mathfrak{S}_j\}_{j=1}^X$  will be governed by a classical effective Hamiltonian  $\tilde{H}(\{\tilde{\mathfrak{S}}_j\}_{j=1}^X)$ . Hence, to predict dynamics of a collective observable  $S(t) = f(\{\mathfrak{s}_j(t)\}_{j=1}^L)$ , we will assume the existence of a function  $\tilde{f}$  of the effective DOFs, which will effectively reproduce the dynamics of  $S(t)$ . Note that, in general,  $\tilde{f}$  is not necessarily of the same functional form of  $f$ . We can then compactly formulate the dynamical reduction hypothesis as

$$\begin{aligned}
 \lim_{L \rightarrow \infty} H(\{\mathfrak{s}_j\}_{j=1}^L) &\xrightarrow{t \gtrsim t^*} \tilde{H}(\{\tilde{\mathfrak{S}}_j\}_{j=1}^X), \\
 \lim_{L \rightarrow \infty} S = f(\{\mathfrak{s}_j\}_{j=1}^L) &\xrightarrow{t \gtrsim t^*} \tilde{f}(\{\tilde{\mathfrak{S}}_j\}_{j=1}^X). \quad (11)
 \end{aligned}$$

The effective Hamiltonian  $\tilde{H}$  is of the same functional form in the integrable case [56,63,105], while it is not generally expected to be so for nonintegrable systems [105]. Importantly, we assume that the effective Hamiltonian obeys the same global symmetries as the many-body Hamiltonian.

In the following, we apply the dynamical reduction hypothesis Eq. (11) to craft various dynamical responses associated to the problem of synchronization in bosonic multilevel cavity QED summarized in Fig. 1. We believe that our conjecture has universal flavor and is applicable to several other settings, as we elaborate further in the concluding section.

### B. Classification of dynamical responses

We construct a classification of dynamical phases by considering the different dynamics collective observables can display in the many-body system. In the case of cavity QED, we consider the magnitude of the intralevel average coherence  $|\Sigma_{n,m}(t)| = |\sum_{j=1}^L \Sigma_{n,m}^{(j)}(t)|/L$  with  $n \neq m$ . These observables can distinguish between cases when the atoms are synchronized ( $|\Sigma_{n,m}(t)| \neq 0$ ) or desynchronized ( $|\Sigma_{n,m}(t)| = 0$ ), and in the case of synchronization we distinguish four dynamical responses.

Desynchronized phase:

(i) Phase I: In the long-time limit  $|\Sigma_{n,m}(t)| \rightarrow 0$ , as a result of classical dephasing processes in the microscopic model due to inhomogeneities in the local fields.

Synchronized phases:

(ii) Phase II:  $|\Sigma_{n,m}(t)|$  relaxes to a stationary nonzero value.

(iii) Phase III:  $|\Sigma_{n,m}(t)|$  displays self-generated Floquet dynamics (i.e., periodic oscillations) characterized by a spectrum with well-resolved commensurate frequencies.

(iv) Phase IV:  $|\Sigma_{n,m}(t)|$  displays aperiodic oscillations characterized by a spectrum with well-resolved incommensurate frequencies.

(v) Phase IV\*:  $|\Sigma_{n,m}(t)|$  displays chaotic oscillations exponentially sensitive to small changes in the initial conditions and characterized by a spectrum with multiple broad peaks.

While phases I and II are quite generic in the presence of inhomogeneous dephasing, phases III, IV, and IV\* are examples of self-generated nonrelaxing responses in the absence of an external drive. As previously mentioned, the

dynamical responses from phase I to phase IV were already observed in the integrable two-level case [56,59,60,77], while the chaotic phase IV\* is accessible only in nonintegrable systems [107].

To predict and control when such phases occur, we use the dynamical reduction hypothesis, and arguments based on symmetry and the Liouville-Arnold theorem. The Liouville-Arnold theorem [108] states that given a system with  $M$  DOFs and  $Q$  conserved quantities, there exists a canonical transformation through action-angle variables, such that  $Q$  actions are constant, and  $Q$  angles evolve periodically at a frequency imposed by the value of the corresponding conserved quantity [108–110]. Thus, if  $2Q \geq M$ , the dynamics is solely along tori and the system is said to be classically integrable. If instead  $2Q < M$ , there will be  $(M - 2Q)$  DOFs which evolve without any constraint and can, in principle, display chaotic behavior. Notice that  $Q \geq 1$  since the effective Hamiltonian always obeys time translation symmetry such that the effective energy is always a conserved quantity.

To apply this theorem to describe the different phases with different effective models, we assume that an  $X$  site effective model has in total  $M$  DOFs. Phase I can be described by an effective model with  $X = 0$  sites, thus  $M = 0$  DOFs, since no effective degree of freedom is necessary to capture a vanishing observable. In the microscopic models, the synchronized phases generally occurs when the all-to-all coupling is large enough with respect to the inhomogeneities in the local fields, and it can be captured by an effective model with  $X \geq 1$  sites, thus,  $M \geq 1$  DOFs, since we need at least one DOF for describing nontrivial behavior. Combining the number of DOFs  $M$ , the number of symmetries  $Q$ , and the number of symmetries under which the specific observable is invariant, it is possible to predict the specific synchronized dynamical response. We show that, in  $SU(N)$  systems, an effective single-site Hamiltonian ( $X = 1$ ) is already sufficient for observing all the dynamical responses from phase I up to phase IV\*. This is in contrast to the  $SU(2)$  integrable case in which an  $X$ -body effective Hamiltonian is necessary to capture phase ( $X + 1$ ) [56,59,60,66,77].

To apply this classification to multilevel cavity QED, we must identify the global symmetries present in such systems and the number of DOFs that could occur in the effective models. We identify the global symmetries and number of DOFs in Sec. III C, present a few examples of effective models in Sec. III D, and give the predictions for the allowed dynamical responses for different  $N$ -level systems in Sec. III E.

### C. Counting DOFs and symmetries

Given a generic product state, as in Eq. (5), we conjecture an effective classical model composed of effective DOFs describing the matter and the cavity field separately. We assume that the effective cavity field is given by a bosonic amplitude  $\tilde{a}$  specified by two real numbers. As the detuning from the atomic transitions increases, the contribution from such DOFs becomes suppressed, and consequently can be neglected in the far detuned limit [66]. The effective matter's DOFs are either  $SU(N)$  spins or bosonic amplitudes, depending on whether the collective observables  $\Sigma_{n,m}(t)$  can be factorized or not.

If  $\Sigma_{n,m}(t)$  cannot be factorized, the emergent effective classical model is composed of  $X$   $SU(N)$ -spins with elements  $\tilde{\Sigma}_{n,m}^{(k)}$  where  $n, m \in [1, N]$  and  $k \in [1, X]$ . Such an effective model has  $M = X \times N^2$  matter DOFs, corresponding to the  $N^2$  matrix elements for each effective spin  $\tilde{\Sigma}^{(k)}$ . Since the effective DOFs are  $SU(N)$  spins, the number of independent parameters is reduced due to the Casimir charges  $\sum_{n=1}^N \tilde{\Sigma}_{n,n}^{(k)}$  and  $\sum_{m=1}^N \tilde{\Sigma}_{n,m}^{(k)} \tilde{\Sigma}_{m,n}^{(k)}$ , which are the conservation of the number of bosons and length of the  $SU(N)$  spin on each site  $k$ . As a consequence, the number of independent matter DOFs is  $M = X \times (N^2 - 2)$ .

Instead, if  $\Sigma_{n,m}(t)$  can be factorized, then the effective model in the  $SU(N)$  spins further simplifies and involves only  $X \times N$  effective bosonic amplitudes  $\tilde{b}_{n,k}$  with  $k \in [1, X]$  and  $n \in [1, N]$ . In this case, the number of matter DOFs is  $M = X \times 2N$ , being each bosonic amplitude specified by two real parameters. Assuming that the effective  $SU(N)$  spins and effective bosons are related analogously to the microscopic ones via  $\tilde{\Sigma}_{n,m}^k = \tilde{b}_{n,k}^* \tilde{b}_{m,k}$ , the two Casimir charges defined above are still conserved. In this case, they are dependent one from the other and can be linked to the local  $U(1)$  symmetry  $\tilde{b}_{n,k} \rightarrow e^{i\phi_k} \tilde{b}_{n,k}$  of the bilinears  $\tilde{b}_{n,k}^* \tilde{b}_{m,k}$ . Since the number of bosons is conserved, the corresponding conjugate variable, the sum of the phases of the bosonic amplitudes, is irrelevant and the number of nontrivial matter DOFs is  $M = X \times (2N - 2)$ .

Once the effective DOFs are identified, we can construct the effective Hamiltonian which governs their dynamics imposing the same symmetries of the many-body Hamiltonian in Eqs. (1) and (2) in the classical limit. The first symmetry is time translation invariance, which implies the conservation of the energy, while the second is a global  $U(1)$  symmetry present solely in absence of corotating processes. Specifically, for  $\lambda_n = 0$  the Hamiltonian in Eq. (1) is invariant under  $(\Sigma_{n,n+1}, a) \rightarrow (e^{i\theta} \Sigma_{n,n+1}, e^{i\theta} a)$  and thus conserves the number of total excitations, which in the two-level case is  $[(\Sigma_{2,2} - \Sigma_{1,1})/2 + |a|^2]$  while in the generic multilevel case is a linear combination of  $\{\Sigma_{n,m}\}$  and  $|a|^2$  [88,111]. Analogously, for  $\nu_{m,n}, \zeta_{n,m} = 0$  the atom-only model in Eq. (2) is invariant under  $\Sigma_{n,n+1} \rightarrow e^{i\theta} \Sigma_{n,n+1}$ , which leads to the conservation of the number of atomic excitations (e.g.,  $(\Sigma_{2,2} - \Sigma_{1,1})$  in the two-level case).

Combining the effective DOFs and symmetries, we can now propose a possible set of effective models and predict the dynamical responses of collective observables via arguments based on symmetry and the Liouville-Arnold theorem.

#### D. Effective models

To make concrete the above picture, here we present a set of possible effective models for multilevel cavity QED systems described by Eq. (1). As mentioned above, an exact derivation is not available in the generic multilevel case (see Refs. [56,63,105], where the effective few-body Hamiltonian can be derived from the Richardson-Gaudin integrability of the  $SU(2)$  case). Nonetheless, considering the initial state to be a generic product state [cf. Eq. (5)], the effective DOFs are  $SU(N)$  spins, and the simplest effective theory is given by the microscopic Hamiltonian in Eq. (1) with  $L = 1$  (thus,  $X = 1$

effective sites)

$$\tilde{H}(\tilde{\Sigma}_{n,m}, \tilde{a}) = \tilde{\omega}_0 \tilde{a}^* \tilde{a} + \sum_{n=1}^N \tilde{h}_n \tilde{\Sigma}_{n,n} + \sum_{n=1}^{N-1} [\tilde{g}_n (\tilde{\Sigma}_{n+1,n} \tilde{a} + \text{H.c.}) + \tilde{\lambda}_n (\tilde{\Sigma}_{n+1,n} \tilde{a}^* + \text{H.c.})]. \quad (12)$$

Analogously, in the far-detuned cavity mode limit described by the Hamiltonian in Eq. (2), we propose the effective Hamiltonian

$$\tilde{H}_e(\tilde{\Sigma}_{n,m}) = \sum_{n=1}^N \tilde{h}_n \tilde{\Sigma}_{n,n} - \sum_{m,n=1}^{N-1} [\tilde{\chi}_{n,m} \tilde{\Sigma}_{n+1,n} \tilde{\Sigma}_{m,m+1} + \tilde{\zeta}_{n,m} \tilde{\Sigma}_{n,n+1} \tilde{\Sigma}_{m+1,m} + \tilde{\nu}_{m,n} \tilde{\Sigma}_{n+1,n} \tilde{\Sigma}_{m+1,m} + \tilde{v}_{m,n} \tilde{\Sigma}_{n,n+1} \tilde{\Sigma}_{m,m+1}]. \quad (13)$$

Additionally, if the collective observables  $\tilde{\Sigma}_{n,m}$  can be factorized, we conjecture effective models for the boson DOFs of the form

$$\tilde{H}(\tilde{b}_n, \tilde{a}) = \tilde{H}(\tilde{\Sigma}_{n,m} = \tilde{b}_n^* \tilde{b}_m, \tilde{a}), \quad (14)$$

$$\tilde{H}_e(\tilde{b}_n) = \tilde{H}_e(\tilde{\Sigma}_{n,m} = \tilde{b}_n^* \tilde{b}_m), \quad (15)$$

where we conjecture that the effective one-body reduced density matrix factorizes as  $\tilde{\Sigma}_{n,m} = \tilde{b}_n^* \tilde{b}_m$ . These effective models are trivially exact when the Hamiltonians in Eqs. (1) and (2) are spatially homogeneous for  $h_n^{(j)} = h_n$  at  $W = 0$ . Indeed, at  $W = 0$  the many-body Hamiltonians trivially reduces to a few-body one due to the permutation symmetry under swapping of any pair of sites. Despite their apparent simplicity, the effective models here introduced allow us to obtain quantitatively the whole set of dynamical responses described in Sec. III B. Furthermore, we show in Sec. V that these models describe correctly the dynamics of collective observables also at moderate inhomogeneity, with a quantitative matching in the case of  $SU(3)$  spin-exchange interactions.

#### E. Classification for multilevel cavity QED

We are now in the position to discuss the possible dynamical phases for the  $X = 1$  effective models introduced in Sec. III D for different number of levels  $N$ . As already anticipated, we consider as collective variable the magnitude of the intralevel average coherences, which in the effective models are given by  $|\tilde{\Sigma}_{n,m}(t)|$  with  $n \neq m$ . The results of this section are summarized in Table I.

For a generic multilevel atom with  $N \geq 4$  levels, the number of DOFs  $M$  is always larger than the  $2Q \leq 4$  symmetries identified. Thus, generically, the effective model can show aperiodic oscillations (phase IV) and may even display chaotic behavior (phase IV\*).

##### 1. $N = 2$ level atoms

The case of  $N = 2$  levels has been well studied [96,112,113] and in this section we discuss how our approach reproduces known results. The number of matter DOFs is  $M = 2$ , either considering an effective bosonic model or with  $SU(2)$  spins. Thus, it is not possible to access different dynamical responses upon introducing quantum correlations

TABLE I. Summary of the dynamical responses of the magnitude of the intralevel average phase coherence captured by the effective Hamiltonians in Eqs. (12) and (13). The number of matter DOFs is either  $(2N - 2)$  or  $(N^2 - 2)$ , depending on whether  $\tilde{\Sigma}$  can be factorized or not, respectively (cf. Sec. III C). If the cavity field detuning  $\tilde{\omega}_0$  is finite, we need two additional DOFs to describe the modulus and phase of the actively participating cavity field. The presence of a U(1) symmetry increases the number of conserved quantities  $Q$  by 1. For the  $N = 3$  spin exchange model (last row), the system can display from phase I to either phase III or phase IV\*, depending on whether  $\tilde{\Sigma}$  can be factorized or not, respectively. In all cases, all the responses with less order than the one reported could be, in principle, accessed tailoring the initial state and the parameters of the Hamiltonian. The same table holds in the case the Hamiltonian is spatially homogeneous, since the effective models are trivially equal to the microscopic ones (cf. Sec. IV).

|   | $Q$ | $N = 2$ | $N = 3$    | $N \geq 4$ |
|---|-----|---------|------------|------------|
| $\tilde{g}, \tilde{\lambda} \neq 0$ and $\tilde{\omega}_0$ finite             | 1   | IV*     | IV*        | IV*        |
| $\tilde{g}, \tilde{\lambda} \neq 0$ and $\tilde{\omega}_0 \rightarrow \infty$ | 1   | III     | IV*        | IV*        |
| $\tilde{\lambda} = 0$ and $\tilde{\omega}_0$ finite                           | 2   | III     | IV*        | IV*        |
| $\tilde{\lambda} = 0$ and $\tilde{\omega}_0 \rightarrow \infty$               | 2   | II      | III or IV* | IV*        |

in the mean-field limits considered. If the cavity field actively participates to dynamics, we need to keep track of two additional DOFs given by the real and imaginary part of its amplitude.

Let us consider the two-level system with a photon actively participating in dynamics. We can identify the two regimes corresponding to either the generalized Dicke model ( $\tilde{\lambda}, \tilde{g} \neq 0$ ) or the Tavis-Cummings model ( $\tilde{\lambda} = 0$ ). Both models have  $M = 4$  DOFs, but a different number of conserved quantities. The generalized Dicke model conserves only the energy beyond the total spin (which we already taken into account), opening the option of chaos (phase IV\*), as seen, for instance, in Refs. [114–122]. Instead, the Tavis-Cummings model has one additional conserved charge (total number of excitations), is therefore integrable, and in fact shows regular dynamics [112,123–125]. Under change to action-angle variables, the dynamics are seen as the evolution on a three-tori, with three independent frequencies. Thus, a general observable might show phase-IV oscillations. Nevertheless, the magnitude of the mean coherence  $|\tilde{\Sigma}_{1,2}(t)|$  only shows periodic oscillations (phase III) since it is invariant under two of the symmetries, specifically the U(1) symmetries  $(\tilde{\Sigma}_{1,2}, \tilde{a}) \rightarrow (e^{i\theta} \tilde{\Sigma}_{1,2}, e^{i\theta} \tilde{a})$  and  $\tilde{b}_n \rightarrow e^{i\theta} \tilde{b}_n$ , with  $n = \{1, 2\}$ , linked to the conservation of the total number of excitations and spin, respectively.

In the limit where the cavity mode is far detuned from the atomic transitions, the Tavis-Cummings model becomes a simple spin-exchange model with  $M = 2Q = 2$  (the conservation of energy and of the total number of excitations are dependent). Since this model can only have two independent frequencies corresponding to the precession of the U(1) angle variables, the observable  $|\tilde{\Sigma}_{1,2}(t)|$  is constant, yielding phase II. If the additional U(1) symmetry is broken, one recovers the Lipkin-Meshkov-Glick (LMG) model, and the observable  $|\tilde{\Sigma}_{1,2}(t)|$  can again oscillate with a single frequency and display phase III, as it is generically observed [99,126–130].

## 2. $N = 3$ level atoms

In the three-level case,  $M$  depends on whether the model reduces to a bosonic model or to a SU(3) spin system. In the bosonic case, the atomic sector is described by  $M = 2N - 2 = 4$  real DOFs. In the generic SU(3) case, the matter is described by  $M = N^2 - 2 = 7$  DOFs. If the photon is an active DOFs, its additional DOFs lead to  $M \geq 6$  in either the bosonic or spin model, and since  $Q \leq 2$  for any set of parameters, the dynamics can enter the chaotic phase IV\*.

The case of the spin-exchange model, corresponding to  $\tilde{\zeta}_{n,m} = \tilde{v}_{n,m} = 0$  in Eq. (13), is perhaps the most interesting, since depending on whether the model reduces to a bosonic model or a SU(3) spin model, the dynamics can be either in phase III or phase IV (possibly IV\*). Indeed, the three-level bosonic model  $\tilde{H}_e(\tilde{b})$  has  $M = 4$  DOFs and  $Q = 2$  conserved charges, corresponding to the total energy and number of excitations  $(\tilde{\Sigma}_{3,3} - \tilde{\Sigma}_{1,1})$ , and is therefore integrable. Again, two of the frequencies are absorbed in the invariance of  $|\tilde{\Sigma}_{n,m}|$  under the two U(1) symmetries, and thus all oscillations must be periodic, yielding phase III. If instead the initial state has  $\tilde{\Sigma}_{nm} \neq \tilde{b}_n^* \tilde{b}_m$ , we must consider the SU(3) spin model  $\tilde{H}_e(\tilde{\Sigma}_{n,m})$ , and the extra number of DOFs leads to  $M > 2Q = 4$ , allowing the dynamics to be either phase IV or phase IV\*. If  $\tilde{\zeta}_{n,m}, \tilde{v}_{n,m} \neq 0$ , the system loses a U(1) symmetry, associated to the conservation of  $(\tilde{\Sigma}_{3,3} - \tilde{\Sigma}_{1,1})$ , and consequently can display chaotic behavior for both bosons or SU(3) spins.

## IV. HOMOGENEOUS SYSTEMS

In this section, we consider the homogeneous case ( $W = 0$ ) of Eq. (2), where the dynamical reduction hypothesis is true due to the permutation symmetry, and we test the predictions of Table I. In Sec. IV A, we consider permutation invariant coherent states, discussing the role of the interactions. In Sec. IV B, we discuss the consequences of classical and quantum correlations in the initial state, focusing on the  $N = 3$  level spin-exchange Hamiltonian, where we observe the onset of a chaotic phase.

For  $W = 0$ , both the Hamiltonians in Eqs. (1) and (2) are permutationally invariant under swapping of any pair of sites, and they can be written as a function of the collective operators in Eq. (4). Thus, we can immediately achieve the thermodynamic limit  $L \rightarrow \infty$  considering a single large SU( $N$ ) spin. As a consequence, in the mean-field limit we exactly obtain the classical Hamiltonians  $\tilde{H}(\tilde{\Sigma}_{n,m}, \tilde{a})$  or  $\tilde{H}_e(\tilde{\Sigma}_{n,m})$ , depending on whether the cavity field is an active DOF or not, respectively. Here, unlike in the general case, the effective DOFs trivially relate to the original collective DOFs being  $\Sigma_{n,m} = f(\tilde{\Sigma}_{n,m}) = \tilde{\Sigma}_{n,m}$ , and the parameters of the effective Hamiltonians are equal to the original ones (e.g.,  $\tilde{\omega}_0 = \omega_0$ ). As discussed in Sec. II B, the choice of reducing the model to spin DOFs, i.e.,  $\tilde{H}_e(\tilde{\Sigma}_{n,m})$ , or to bosons,  $\tilde{H}_e(\tilde{b}_n)$ , depends only on the purity of the effective one-body reduced density matrix  $\tilde{\Sigma}$ , i.e., whether its elements  $\tilde{\Sigma}_{n,m}$  can be factorized as the product of bosonic operators. In the next sections, we investigate both scenarios and confirm the prediction summarized in Table I.

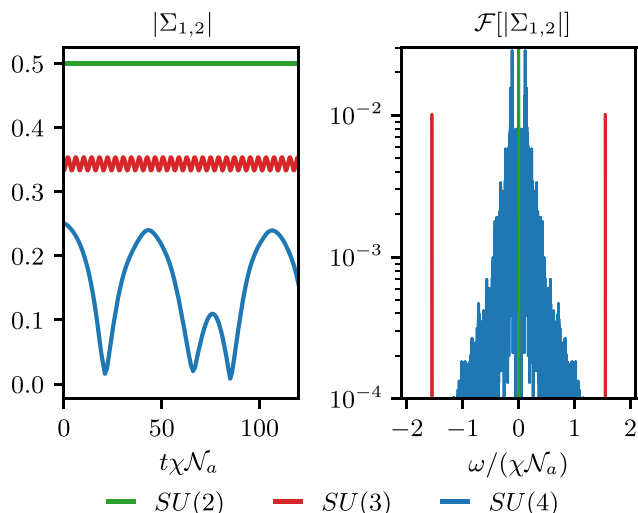


FIG. 3. Left plot: Dynamics of the magnitude of the average phase coherence  $|\Sigma_{1,2}(t)|$  in the homogeneous limit ( $W = 0$ ) for the  $N$ -level spin-exchange model [Eq. (2) with  $v_{n,m} = \zeta_{n,m} = 0$ ] with  $N = \{2, 3, 4\}$ . The initial state is a permutation invariant (in space) coherent state with the same average occupation on each level  $n \in [1, N]$ . The couplings  $\chi_{n,m}$  are chosen such that we have genuine  $SU(N)$  spins. For  $N = 2$ ,  $|\Sigma_{1,2}(t)|$  is constant (phase II); for  $N = 3$ ,  $|\Sigma_{1,2}(t)|$  displays periodic oscillations (phase III); for  $N = 4$ , there are not enough conserved quantities to constrain the space of accessible states and therefore  $|\Sigma_{1,2}(t)|$  displays oscillations exponentially sensitive to small changes in initial conditions (phase IV\*). Right plot: Magnitude of the Fourier spectrum of  $|\Sigma_{1,2}(t)|$ . For  $N = 2$ , the only nonzero component is at  $\omega = 0$ , being  $|\Sigma_{1,2}(t)|$  a constant; for  $N = 3$ , the spectrum has two well-resolved peaks; for  $N = 4$ , there are multiple broad peaks. Due to the permutation invariance under swapping of any pair of sites, the thermodynamic limit can be achieved by simulating a single site ( $L = 1$ ) in the microscopic model in Eq. (2) or, equivalently, the effective model of Eq. (15).

### A. Homogeneous coherent states

We set as the initial state a permutationally invariant (in space) coherent state with equal average occupation on each level  $|\gamma_{n,j} = \gamma$  in Eqs. (8)]. Since the state is homogeneous in space, the average one-body reduced density matrix is pure and can be factorized in the bosonic amplitudes as  $\Sigma_{m,n} = b_m^* b_n$ . Therefore, the effective model describing collective observables is either  $\tilde{H}(b_n, a)$  or  $\tilde{H}_e(b_n)$  (notice that we interchanged the effective bosonic amplitudes with the microscopic ones being equal in this case). We show results only in the case where the photon is not an active DOF. Generally, we expect that an active photon leads to a change of dynamical response from phase  $Y$ , displayed in its absence, to phase  $(Y + 1)$ , due to the additional DOFs [66]. Nonetheless, this effect is suppressed as the detuning of the cavity field frequency with respect to the atomic transitions increases, making our results approximately valid also for large but finite detunings.

In Fig. 3, we show the dynamics of the magnitude of the phase coherence  $|\Sigma_{1,2}|$  in the spin-exchange model [Eq. (2) with  $v_{n,m} = \zeta_{n,m} = 0$ ] in the homogeneous limit ( $W = 0$ ) for different number of atomic levels  $N \in \{2, 3, 4\}$ . As predicted in Table I, upon changing the number of levels, the system can

display markedly different dynamical responses: for  $N = 2$ ,  $|\Sigma_{1,2}|$  displays phase II; for  $N = 3$ ,  $|\Sigma_{1,2}|$  displays phase III; for  $N = 4$ ,  $|\Sigma_{1,2}|$  displays chaotic behavior (phase-IV\*). We also observe the onset of aperiodic oscillations (phase IV) in the  $N = 4$  case for different sets of parameters and initial states. This is a simple signature of the importance of considering multilevel atoms, although the model has all-to-all interactions.

### B. Chaos induced by quantum correlations

In this section, we discuss the impact of quantum correlations in the initial state in the spin-exchange model [Eq. (2) with  $v_{n,m} = \zeta_{n,m} = 0$ ]. We show that the subsequent dynamics is susceptible to quantum correlations, with particularly striking effects in the  $SU(3)$  case, where we can craft a specific dynamical response by manipulating the initial state, from phase III up to phase IV\* (chaos).

We set on each site the same multimode Schrödinger cat state [cf. Eq. (10)]. As discussed in Sec. II C, when  $|\langle \tilde{\gamma}^{(1)} | \tilde{\gamma}^{(2)} \rangle| < 1$ , the one-body reduced density matrix is mixed, the phase coherences do not factorize ( $\Sigma_{n,m} \neq b_n^* b_m$ ), and we have to keep track of all the bilinears  $\Sigma_{n,m}$ . Thus, the effective model passes from the one in the bosonic DOFs defined in Eq. (15) to the one in the  $SU(N)$  spins defined in Eq. (13). Due to quantum correlations, the number of effective DOFs passes from  $2N$  to  $N^2$  and the constraint imposed by the conserved quantities no longer ensures classical integrability for  $N > 2$ . This is particularly striking in the  $SU(3)$  case, where quantum correlations in the initial state can lead to a transition from a regular regime to a chaotic one. For this reason, we focus on the  $SU(3)$  case in the following. Specifically, we consider as initial state a family of multimode Schrödinger cat state [cf. Eq. (10)] parameterized via a parameter  $p \in [0, 1/3]$  as

$$\begin{aligned} \mathcal{Y}^{(1)} &= \sqrt{\frac{\mathcal{N}_a}{L}} \cdot (\sqrt{1/3 + p}, \sqrt{1/3}, \sqrt{1/3 - p}), \\ \mathcal{Y}^{(2)} &= \sqrt{\frac{\mathcal{N}_a}{L}} \cdot (\sqrt{1/3}, \sqrt{1/3 - p}, \sqrt{1/3 + p}). \end{aligned} \quad (16)$$

The overlap  $|\langle \tilde{\gamma}^{(1)} | \tilde{\gamma}^{(2)} \rangle|$  is exponentially suppressed both in  $p$  and  $\mathcal{N}_a/L$ , so  $\langle \tilde{\gamma}^{(1)} | \tilde{\gamma}^{(2)} \rangle = 0$  for any  $p > 0$  in the limit  $\mathcal{N}_a/L \rightarrow \infty$ . We quantify quantum correlations by the connected two-point functions ( $\Sigma_{n,m} - b_n^* b_m$ ). Given the state in Eq. (16), the connected two-point functions are null at  $p = 0$  and increase polynomially with  $p$ . As a consequence, the number of effective DOFs  $M$  needed is expected to increase with  $p$ . Based on our classification, we thus expect a change of the collective dynamical response displayed. This is manifest looking at the Fourier spectrum of  $|\Sigma_{1,2}|$  [cf. Fig. 4(a)], where as  $p$  increases we observe a crossover from a regime with few commensurate peaks (phase III) to a regime with multiple incommensurate one (phase IV), analogous to period doubling phenomena, and eventually the onset of chaos (phase IV\*) for  $p \gtrsim p^*$ . The value  $p^*$  generally depends on the parameters of the Hamiltonian. We locate  $p^*$  computing the maximum Lyapunov exponent  $\sigma$ , which is the largest exponential rate at which nearby trajectories diverge and it is finite and positive in chaotic system and zero for regular Hamiltonian dynamics

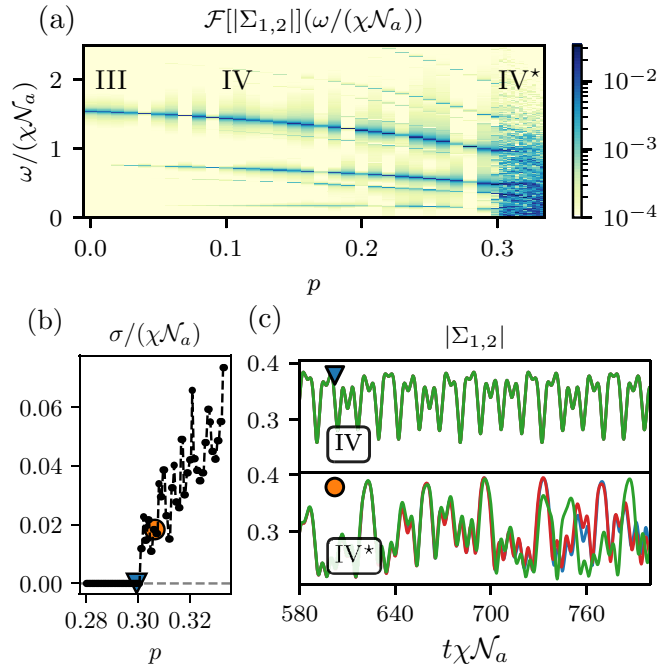


FIG. 4. Dynamical response in the  $N = 3$  level spin-exchange model starting from a multimode Schrödinger cat state [cf. Eq. (16)] as a function of initial quantum correlations parameterized via  $p$ . We set  $\mathcal{N}_a \rightarrow \infty$ ,  $g_1/g_2 \approx 2$ , and  $W = 0$ . (a) Magnitude of the Fourier spectrum of the magnitude of the average coherence  $|\Sigma_{1,2}|$  (the other  $|\Sigma_{n,m}|$  behaves similarly) as a function of  $p$ , which displays a crossover from few commensurate peaks (phase III) to a regime with multiple incommensurate ones (phase IV), and eventually signals the onset of a chaotic phase (phase IV\*). (b) Maximum Lyapunov exponent  $\sigma/(\chi\mathcal{N}_a)$  as a function of  $p$ , which enables us to locate the transition from a regular regime to a chaotic one at  $p^* \approx 0.3$ . (c) Dynamics of  $|\Sigma_{1,2}(t)|$  starting from three nearly sampled initial states at two different values of  $p \approx \{0.299, 0.306\}$  [marked in (b)], showing exponential sensitivity to changes in initial conditions in phase IV\*.

[131,132]. We find  $p^* \approx 0.3$  for  $g_1/g_2 \approx 2$  [cf. Fig. 4(b)]. We refer to Appendix A for the details of the calculation of the Lyapunov exponent and  $p^*$ .

We highlight that the interactions between SU(3) spins are an essential ingredient for observing chaos. Indeed, for  $g_1 = g_2$  (and thus  $\chi_{1,1} = \chi_{2,2} = \chi_{1,2}$ ), dynamics take place in a SU(2) subgroup of SU(3), thus the number of DOFs reduces and there cannot be chaos as a consequence of the Arnold-Liouville theorem. While deep in the SU(3) regime we have chaos for any  $p \gtrsim p^*$ , instead near the SU(2) limits we observe regions in  $p$  of chaotic behavior embedded in regular ones (specifically, phase IV). In Appendix B, we provide details on the Lyapunov exponent as a function of  $p$  and the ratio  $g_1/g_2$ , passing from the SU(2) ( $g_1 = g_2$ ) to the SU(3) spin case ( $g_1 \neq g_2 \neq 0$ ).

In the absence of interference effects ( $\langle \tilde{\gamma}^{(1)} | \tilde{\gamma}^{(2)} \rangle = 0$ ), as it is for any  $p > 0$  in the limit  $\mathcal{N}_a/L \rightarrow \infty$  considered, the equations of motion of the collective observables  $\Sigma_{n,m}$  are the same starting either from the Schrödinger cat state in Eq. (10) or from a state with half sites in the state  $|\tilde{\gamma}^{(1)}\rangle$  and the other half in the state  $|\tilde{\gamma}^{(2)}\rangle$ . In this context,  $p$  effectively controls

the ‘sharpness’ of a ‘kink’ in the initial spatial configuration of the SU(3) spins, in analogy with domain walls in the SU(2) case [77]. The primary difference is that in Ref. [77] it is only possible to generate phase III by considering an inhomogeneous configuration of the local fields. Specifically, they consider a configuration such that the local fields are positive in half the sites and negative in the other half, and initializing the  $z$  component of the spins along their corresponding local field, which is equivalent to a spatial kink. In analogy, we can notice that embedding a Schrödinger cat state is similar to the insertion of an internal quantum kink: the word quantum highlights the presence of multiparticles entangled states, while kink refers to the phase-space representation of the state, which would be given by two coherent states pointing in opposite directions, but now in the internal Hilbert space of the atom.

The sharp feature in the Lyapunov exponent as a function of  $p$  in Fig. 4(b) looks similar to a first-order phase transition. A field theory investigation of this phenomenon is ongoing and it represents a natural and fruitful direction of outreach of our results.

### C. Chaotic seeds in initial states

We now explore the option to induce a chaotic phase by initializing a fraction of the sites in a Schrödinger cat state, while keeping the other sites in a coherent state. We consider  $|\psi_{\text{cat}}\rangle \sim (|\tilde{\gamma}^{(1)}\rangle + |\tilde{\gamma}^{(2)}\rangle)$  as defined in Eq. (16) with  $p \in [0, 1/3]$ . We initialize a fraction  $F \in [0, 1]$  of sites in  $|\psi_{\text{cat}}\rangle$  such that the initial state is

$$|\Psi\rangle = \otimes_{j=1}^{\lfloor FL \rfloor} |\psi_{\text{cat}}\rangle \otimes_{j=\lfloor FL \rfloor+1}^L |\tilde{\gamma}^{(1)}\rangle, \quad (17)$$

where  $\lfloor x \rfloor$  returns the least integer greater than or equal to  $x$ . The region initialized in  $|\psi_{\text{cat}}\rangle$  could favor phase IV\*, while the region initialized in a coherent state would favor a regular dynamical response (phase III). We observe that the chaotic region proliferates and drives the whole system into the chaotic phase IV\* for  $F \gtrsim F^*$ , where  $F^*$  depends on the details of the initial state and parameters of the Hamiltonian. For the state in Eq. (17),  $F^* \approx 0.5$  at  $p \approx 1/3$ . In Appendix C, we offer a more detailed analysis.

## V. EFFECTS OF INHOMOGENEOUS FIELDS

Upon introducing inhomogeneous local fields ( $W > 0$ ), the permutation symmetry is broken and the Hamiltonians in Eqs. (1) and (2) cannot be straightforwardly written as a function of collective DOFs. Regardless, the dynamical responses observed in the homogeneous case ( $W = 0$ ) are generally robust against finite inhomogeneity ( $W > 0$ ), and we provide numerical evidence that the simple effective Hamiltonians defined in Sec. III D describe quantitatively the many-body collective dynamics of the full model in a regime of moderate inhomogeneity  $W$ . In particular, we focus on the spin-exchange Hamiltonian in Eq. (2) for  $v_{n,m} = \zeta_{n,m} = 0$ :

$$H = \sum_{j=1}^L \sum_{n=1}^N h_n^{(j)} \Sigma_{n,n}^{(j)} - \sum_{m,n=1}^{N-1} \chi_{n,m} \Sigma_{n+1,n} \Sigma_{m,m+1}. \quad (18)$$

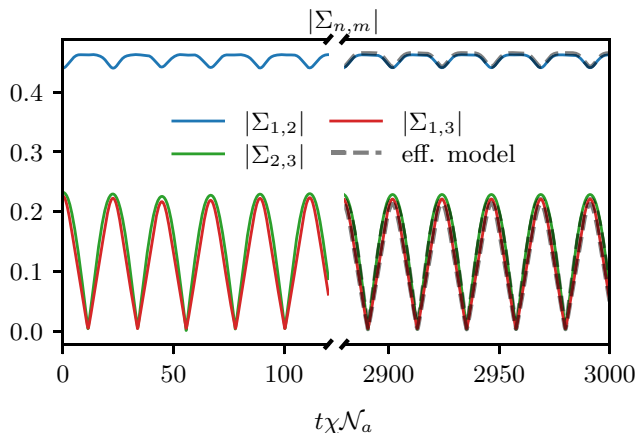


FIG. 5. Dynamics of the magnitude of the average phase coherence  $|\Sigma_{m,n}(t)|$  in the  $N = 3$  level spin-exchange model at fixed  $g_2/g_1 \approx 10^{-2}$  and  $W/(\chi\mathcal{N}_a) = 0.1$ . The initial state is a permutationally invariant (in space) coherent state. The continuous lines are obtained simulating the full many-body dynamics with  $L = 10^4$  sites. The dashed black lines are obtained simulating the effective model in Eq. (13) with parameters numerically obtained by the optimization of the cost function in Eq. (19).

To demonstrate the validity of the effective Hamiltonian, we numerically identify the parameters of the simple *ansatz* in Eq. (13) that reproduce the dynamics of collective observables. Our procedure can be summarized as follows:

(i) We compute the time evolution of the collective observables  $\Sigma_{n,m}(t)$  from the full many-body dynamics obtained via the Hamiltonian in Eq. (18).

(ii) We set the initial conditions  $\{\tilde{\Sigma}_{n,m}(t=0)\}$  and give a numerical seed to the parameters  $\{\tilde{h}_n, \tilde{\chi}_{n,m}, \tilde{\zeta}_{n,m}, \tilde{v}_{n,m}\}$  in the effective model in Eq. (13).

(iii) We compute the time evolution of the collective observables using the effective model in Eq. (13).

(iv) We vary the initial conditions and effective Hamiltonian parameters to minimize the average norm-1 distance between  $\Sigma(t)$  computed in (i) and  $\tilde{\Sigma}(t)$  computed using the effective model in (iii), i.e., we set as cost function

$$\epsilon_1 = \frac{1}{T} \int_0^T \sum_{n,m=1}^N |\tilde{\Sigma}_{n,m}(t) - \Sigma_{n,m}(t)| dt. \quad (19)$$

In Appendix D, we discuss the details of steps (ii) and (iv).

Since the dynamical reduction hypothesis has been extensively demonstrated to hold exactly for two-level atoms through integrability [56,63,105], we focus on the  $N = 3$  level case. In Fig. 5, we show the results obtained in the spin-exchange model at  $W/(\chi\mathcal{N}_a) = 0.1$  by simulating the full many-body dynamics given by Eq. (18) (continuous line). We initialize the system in a permutation invariant coherent state [cf. Eqs. (8)] which displays phase III at  $W = 0$ , and we consider photon-matter couplings  $g_1 \neq g_2$ , so  $\chi_{1,1} \neq \chi_{2,2} \neq \chi_{1,2}$  in Eq. (18). The black dashed lines are obtained from the numerically optimized single-body effective Hamiltonian. The dynamics of collective observables obtained via the effective Hamiltonian match well the dynamics obtained via the full many-body mean field Hamiltonian; this suggests not only

that the dynamical response observed in the homogeneous case is robust but also that the dynamical reduction hypothesis holds at finite  $W$ .

Due to exponential sensitivity to initial conditions, the procedure described above does not converge with high enough accuracy in the SU(3) system in the chaotic phase of Sec. IV B, which, however, persists also for weak inhomogeneities.

#### A. Robustness of dynamical responses to inhomogeneities

Inhomogeneities in the local fields are generally expected to have an impact on the dynamics of collective observables. One could argue that for  $W/(\chi\mathcal{N}_a) \gg 1$  the local fields  $\{h_n^{(j)}\}$  will dominate dynamics, and phase coherences would be washed out (phase I). Here, we explore the dynamical responses at moderate inhomogeneity in the spin-exchange Hamiltonian of Eq. (18) for  $N = 3$  and  $N = 4$  level atoms. In the  $N = 3$  level case, we initialize a multimode Schrödinger cat state on each site for which the dynamical response is chaotic (phase IV\*) at  $W = 0$ . On the contrary, in the  $N = 4$  level case, we consider a coherent state for which the dynamical response is aperiodic (phase IV) at  $W = 0$ . In both cases,  $|\Sigma_{n,m}|$  displays dynamical responses different from phase I and phase II (relaxation) for  $W/(\chi\mathcal{N}_a) \lesssim 1$ .

First, let us consider the  $N = 4$  spin-exchange model in Eq. (18). In Fig. 6, we show the dynamics of  $|\Sigma_{2,3}|$  for different values of inhomogeneity  $W/(\chi\mathcal{N}_a)$ . We fix as the initial condition a permutation invariant (in space) coherent state with different amplitudes on each level. The intralevel phase coherences  $|\Sigma_{n,m}|$  displays phase IV up to a finite value of inhomogeneity  $W/(\chi\mathcal{N}_a)$ . Upon increasing  $W/(\chi\mathcal{N}_a)$ ,  $|\Sigma_{n,m}|$  displays phase III, phase II, and eventually phase I. The different dynamical responses are divided by regions (not shown in Fig. 6) where the distinction between the different dynamical responses becomes more blurry.

Similarly, in the SU(3) case, the dynamical response generally passes from phase  $Y$  to phase  $(Y - 1)$  as  $W/(\chi\mathcal{N}_a)$  is increased (at fixed initial state), and with the dynamics eventually entering phase I due to the dominant inhomogeneous local fields (bottom panels in Fig. 7). Instead, as initial quantum correlations in the initial state increase with  $p$ , the dynamical response generally passes from phase  $Y$  to phase  $(Y + 1)$  (top panels in Fig. 7). Additionally, we highlight that the dynamical responses are generally robust against small breaking of the permutation symmetry in the initial state.

The robustness of the various dynamical responses against inhomogeneous local fields for  $W > 0$  can be ascribed to the many-body gap  $\propto \chi\mathcal{N}_a$  that suppresses local spin flips and favors spin alignment. This mechanism has been shown to protect phase coherence in the spin-exchange model between SU(2) spins [18,50,133] and is likely present also in our  $N$ -level case. As  $W$  increases, this many-body gap protection is less effective and dephasing processes between the SU( $N$ ) take over. As a result, within the framework of the dynamical reduction hypothesis, the number of effective sites required to describe dynamics is reduced and accordingly the dynamical responses change.

For instance, in the SU(4) case (cf. Fig. 6), at moderate inhomogeneity the system has  $M > 2Q$  effective DOFs, which

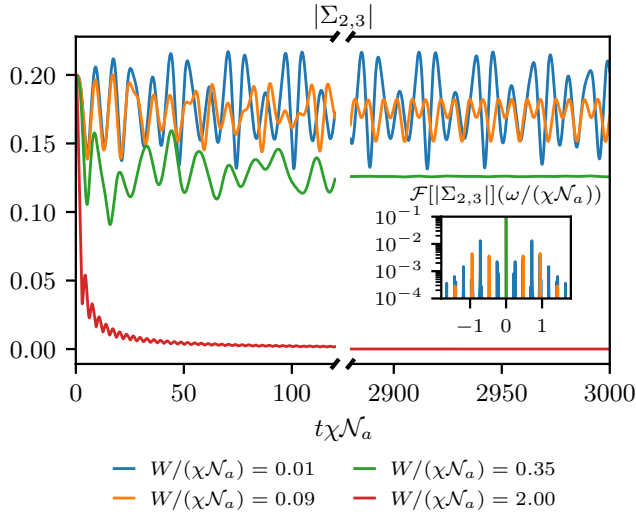


FIG. 6. Dynamics of the magnitude of the average phase coherence  $|\Sigma_{2,3}(t)|$  in the  $N = 4$  level spin-exchange model for  $\chi_{1,2} \neq \chi_{2,3} \neq \chi_{3,4}$ . The initial state is a permutation invariant (in space) coherent state. As  $W/(\chi N_a)$  increases, the system displays different dynamical responses, passing from phase IV to phase III, then to phase II and eventually to phase I. The different phases are separated by crossover regions where the dynamical responses cannot be sharply identified (not shown here). In the inset, we show the magnitude of the Fourier spectrum in the late time dynamics. The results shown are obtained with  $L = 10^4$  sites and are not appreciably affected upon increasing  $L$ .

lead to to phase IV observed in the  $W = 0$  case. As  $W$  becomes sizeable, dephasing starts to affect dynamics and, since  $M \leq 2Q$ , the system displays phases III, II, and eventually I, upon increasing the degree of inhomogeneity. The effects of dephasing are apparent in the Fourier spectrum of  $|\Sigma_{n,m}(t)|$  (cf. inset of Fig. 6), where the various Fourier components are depleted as  $W$  increases until the whole spectrum becomes flat in phase I. Similarly, in the SU(3) case, inhomogeneity leads to a loss of effective phase-space, a reduction of the effective DOFs and, correspondingly, leads to a loss of chaos (the Lyapunov exponent vanishes). Along the same argument, the number of effective DOF  $M$  increases as initial correlations in the initial state increase, thus the system could enter in a regime with different dynamical responses and eventually display chaotic behavior, as observed in the homogeneous case of Fig. 4. We highlight that the dynamical response displayed does not necessarily have to pass smoothly from phase  $Y$  to phase  $(Y \pm 1)$ , but there can be a jump, as in the SU(3) case where phase IV turns into phase I (see Fig. 7), without displaying phases III and II. This has been also reported in the integrable SU(2) case [77].

## VI. EXPERIMENTAL IMPLEMENTATION

A possible experimental scheme to implement the couplings of Hamiltonian Eq. (2) is sketched in Fig. 8. Ensembles of  $N_a/L$  atoms are trapped at  $L$  fixed positions and collectively coupled to a single mode of a high finesse optical cavity with resonance frequency  $\omega_c$ . At the same time, the atoms are subject to a multifrequency laser field. The atoms are

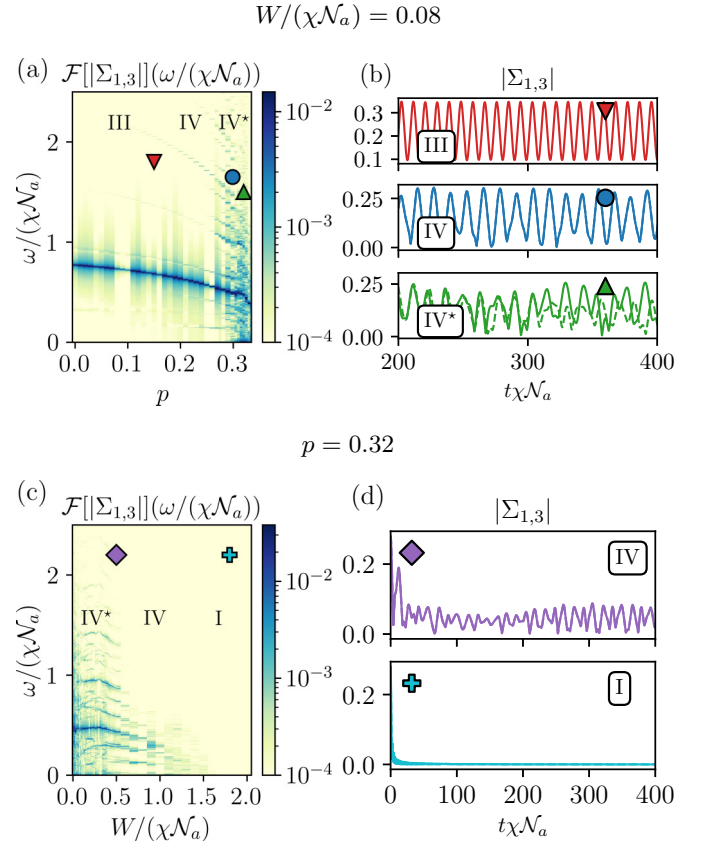


FIG. 7. Dynamical response in the  $N = 3$  level spin-exchange model [Eq. (18)] with inhomogeneity  $W/(\chi N_a)$  and  $g_1/g_2 \approx 2$  ( $\chi_{1,1} \neq \chi_{1,2} \neq \chi_{2,2}$ ), initializing a multimode Schrödinger cat state parameterized by  $p$  [cf. Eq. (16)] on each site. We focus on  $|\Sigma_{1,3}|$ ; the other phase coherences behave similarly. In the top panels, we show the magnitude of the Fourier spectrum and dynamics of  $|\Sigma_{1,3}|$ , starting from two close-by initial states, changing  $p$  at fixed  $W/(\chi N_a) = 0.08$ . Instead, in the bottom panels we change  $W/(\chi N_a)$  keeping  $p = 0.32$  fixed. As  $p$  increases, and  $W/(\chi N_a)$  is fixed, we can infer from the Fourier spectrum in (a) crossover from a regime with well-resolved peaks with commensurate frequencies (phase III) to multiple peaks with incommensurate frequencies (phase IV) and eventually to spectrum with multiple broad peaks typical of chaotic dynamics (phase IV\*). In (b), we show three examples of the different dynamical responses at  $p = \{0.15, 0.299, 0.32\}$  (marked in the plot of the Fourier spectrum). As  $W/(\chi N_a)$  increases, the system passes from phase IV\* to phase IV and eventually phase I. In the (d) panel, we show the dynamics at  $W/(\chi N_a) = \{0.5, 1.8\}$ , corresponding to phases IV and I (marked in the plot of the Fourier spectrum), respectively. The results shown are obtained with  $L = 10^4$  sites and are not appreciably affected upon increasing  $L$ .

assumed to have a manifold of ground-state sublevels which can be coupled using Raman transitions. If one leg of such a Raman transition is driven by a classical field while the second leg is coupled to the resonator mode, cavity-assisted Raman transitions can be implemented [20,37,38]. In a microscopic description, a photon from the laser field is scattered into the cavity, while the internal state of an atom in one of the ensembles is changed. The photon is delocalized over the cavity mode and can subsequently drive a second Raman transition

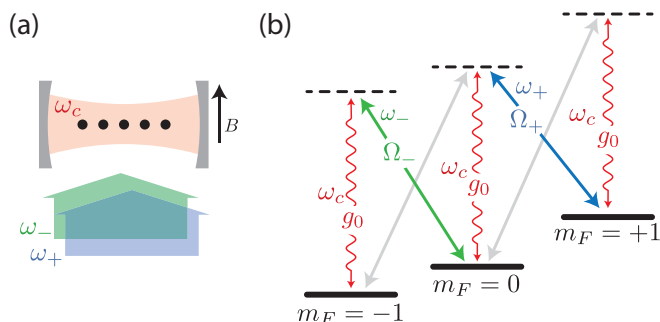


FIG. 8. Suggested experimental implementation. (a) Ensembles of 3-level atoms in  $L$  traps (black dots) are coupled to a single mode of an optical cavity (red) and transversely illuminated by a two-frequency laser field (blue, green). (b) The applied magnetic field  $B$  leads to a non-degenerate atomic level splitting allowing to selectively drive cavity-assisted Raman transitions. Coupling via the transverse laser fields (the cavity) are shown as solid (wiggly) arrows. If additional frequency components (grey arrows) are introduced, co- and counter-rotating terms can be engineered.

in another atomic ensemble. In this process, the photon is absorbed by an atom and then emitted into the driving laser field via bosonic stimulation.

As an example, we consider  $^{87}\text{Rb}$  atoms, where the  $F = 1$  ground-state hyperfine manifold has  $N = 3$  magnetic sublevels  $m_F = (0, \pm 1)$ . A sufficiently strong applied magnetic field leads to a nondegenerate level splitting due to linear and quadratic Zeeman shifts, as sketched in the figure. In combination with a two-frequency transverse laser field, this allows us to drive state-selective, cavity-assisted two-photon Raman transitions between these states, as indicated in Fig. 8(b). The laser field is far detuned from atomic resonance to avoid any spontaneous decay of the excited atomic state. The frequencies  $\omega_+$  and  $\omega_-$  of the transverse laser field are chosen to match the different atomic level splittings when a photon is absorbed from or emitted into the cavity mode. For example, an atom at a specific site can be transferred from  $m_F = 0$  to  $m_F = -1$  by absorbing a photon from the laser field at frequency  $\omega_-$  and emitting a photon into the cavity. The very same cavity photon can then drive a transition at a different site where an atom in  $m_F = 0$  absorbs that photon and undergoes a transition to  $m_F = +1$  while emitting into the laser field at frequency  $\omega_+$ . These two-photon Raman transitions correspond to the processes proportional to  $g_n$  in Hamiltonian Eq. (2), where the coupling strengths  $g_n$  can be engineered via the single-photon Rabi frequencies  $\Omega_+$  and  $\Omega_-$ .

The corotating terms proportional to  $\lambda_n$  in Hamiltonian Eq. (2) can be implemented if additional laser frequencies are added to the transverse laser field. Such couplings are indicated by the grey arrows in Fig. 8(b). The relative strengths of the co- and counterrotating terms can be independently tuned via the respective Rabi rates of the driving laser fields [38].

This scheme can further be extended to  $N > 3$  by choosing atomic states with larger magnetic sublevel manifolds as can be found, for example, in lanthanide atoms. Finally, site-dependent energies  $h_n^{(j)}$  of the atomic modes can be introduced by applying a magnetic-field gradient along the cavity axis

in addition to the homogeneous magnetic field [40,134]. In a realistic scenario, also cavity decay due to losses at the mirrors has to be taken into account. Its influence can, however, be reduced by introducing a detuning between the cavity resonance and the frequency of the field scattered into the cavity mode.

## VII. DISCUSSION

### A. Role of dissipation

In our analysis, we have considered the system completely isolated from the environment. In cavity-QED systems, there are two main sources of dissipation, free-space emission of single-atom excitations and loss of the cavity field. Let us denote the rates of the two processes with  $\eta$  and  $\kappa$ , respectively, and their jump operators with  $\hat{L}_n^{(j)} = \sqrt{\eta} \hat{\Sigma}_{n,n+1}^{(j)}$  and  $\hat{L} = \sqrt{\kappa} \hat{a}$ , where  $j \in [1, L]$  and  $n \in [1, N - 1]$ . The relevant timescales for the coherent dynamics are set by the collective photon-matter couplings  $\lambda_n \sqrt{\mathcal{N}_a}$  and  $g_n \sqrt{\mathcal{N}_a}$ . The different dynamical responses can be dominantly ascribed to Hamiltonian dynamics if  $\lambda_n \sqrt{\mathcal{N}_a}, g_n \sqrt{\mathcal{N}_a} \gg \kappa, \eta$ .

We provide a more accurate estimate in the far detuned cavity mode regime, where all the results of this paper have been derived. Focusing on the  $\text{SU}(N)$  spin-exchange case for simplicity, the photon effectively induces elastic all-to-all interactions of strength  $\chi_{n,m} = g_n g_m \omega_0 / (\omega_0^2 + (\kappa/2)^2)$ ; in addition, the collective atomic transitions are radiatively broadened by the coupling to the cavity, leading to collective decays with rate per-atom  $\Gamma_n = g_n^2 \kappa / (\omega_0^2 + (\kappa/2)^2)$  [135–139]. The coherent dynamics are fast with respect to the timescales of the dissipation if  $\mathcal{N}_a \chi_{n,m} \gg \{\mathcal{N}_a \sqrt{\Gamma_n \Gamma_m}, \eta\}$ , which translate to  $\omega_0 \gg \kappa$  and  $\mathcal{N}_a \chi_{n,m} \gg \eta$  (see Appendix E for the complete derivation). In this parameter regime, dynamics are basically ruled only by coherent evolution, at least up to times parametrically large in  $\omega_0/\kappa$  and  $\mathcal{N}_a \chi_{n,m}/\eta$ .

### B. Connection with $\text{SU}(N)$ fermionic systems

As already anticipated in Sec. II C, the number of atoms per site  $\mathcal{N}_a/L$  is a conserved quantity in our system and our results can be extended to a large class of systems which can be mapped to the Hamiltonians in Eqs. (1) and (2). As an example, let us consider an  $N$ -level fermionic system with annihilation (creation) operators  $\hat{c}_{n,j}^{(\dagger)}$  with  $n \in [1, N]$  and site index  $j$ . We can define the pseudospins  $\hat{\Sigma}_{n,m}^{(j)} \equiv \hat{c}_{n,j}^\dagger \hat{c}_{m,j}$  [92], which in turn can be expressed in terms of Schwinger bosons as  $\hat{\Sigma}_{n,m}^{(j)} = \hat{b}_{n,j}^\dagger \hat{b}_{m,j}$ . If via this procedure the fermionic Hamiltonian as a function of the Schwinger bosons is identical to one of the Hamiltonians here investigated, our results obtained via coherent states could be applied straightforwardly. Indeed, the mean field at the level of the Schwinger bosons is mathematically equivalent to simulating pure single-particle states  $|\psi_j\rangle = \sum_{n=1}^N \langle \hat{b}_{n,j} \rangle |n_j\rangle$ , with the caveat of interpreting the bosonic amplitudes as probability amplitudes [51].

### C. Roadway towards a universal dynamical reduction hypothesis

In this paper, we have formulated and tested a reduction hypothesis for the dynamics of  $\text{SU}(N)$  cavity QED systems with atoms in a multilevel ladder configuration. We found

that the reduction hypothesis was a useful description for a variety of systems with different initial states, levels, inhomogeneous fields, and light-matter interactions. This plethora of applications calls naturally for a broader framework. Our classification of dynamical responses based on the dynamical reduction hypothesis and the Arnold-Liouville theorem might possess the flavor of universality. It would be, in fact, extremely interesting to encompass all the specific examples mentioned above, under the lenses of the symmetries both of the local DOFs and of the light-matter interactions. Similarly to renormalization group approaches, one could explore the basins of attraction of the effective few-body models presented here. Upon changing the symmetries and the conservation laws of a given macroscopic model, one could expect to distinguish a set of irrelevant perturbations in which the reduction hypothesis remains valid, and set of relevant perturbations in which the reduction hypothesis fails and no effective few-body model describes the dynamics of collective observables.

From our numerical experiments, it seems natural that perturbations that do not dramatically change the long-range nature of the interactions would be irrelevant. We would therefore expect similar dynamical responses in the presence of different photon-assisted transitions (e.g., from the  $n$ th level to any  $m$ th level via a single-photon process) or of squeezed terms [e.g.,  $\propto (b^\dagger b^\dagger a + \text{h.c.})$ ], where the information about the state cannot be retrieved solely by the  $SU(N)$  coherences but would also require terms such as  $\langle b^\dagger b^\dagger \rangle$  [39]. Investigations into the latter perturbations might disclose connections between multimode squeezing and the generation of universal dynamical responses. It is also completely natural to investigate the impact of different level configurations, for instance, studying the case of two degenerate subspaces of excited and ground states [43,44,140]. A preliminary analysis suggests that they are also irrelevant perturbations and that a reduction hypothesis still holds here. Finally, we note that  $SU(N)$  generalizations of BCS models [79–82] would, under a generalized Anderson pseudospin mapping, have a similar form as to the models we study here and also be describable by a reduction hypothesis.

In contrast, any perturbation that introduces short-range interactions could be expected to be relevant to the effective few-body Hamiltonian basin of attraction. This appears to be the case in the context of time crystals [41,42,141–144], where short-range interactions generally melt the time crystal at late times and lead to generically asynchronous relaxation. Separability of the interactions will also likely play a role: systems with separable interactions seem describable by an effective few-body model [66,145]; while models with inseparable interactions can lead to glassy relaxation [146–148] and cannot be described by effective few-body models [145,149]. Furthermore, systems with a number of atomic levels comparable to the number of sites,  $N \sim L$ , may also pose obstacles in defining an effective few-body theory but could be relevant for experiments in synthetic dimensions [83,84]. Naturally, the effects of dissipation would also not be captured by a few-body Hamiltonian picture but instead potentially be described by a few-body dissipative model such as a Lindblad master equation.

The strong numerical-oriented approach we have taken here has provided serious evidence of a description using an

effective few-body model, even demonstrating a near-perfect ability to capture the dynamics of collective observables. Still, an analytic approach could yield important insights and provide a more solid ground for classifying different perturbations as relevant or irrelevant to the few-body attractive basin. Considering the variety of AMO systems modeled by collective interactions, finding such a description would constitute a significant step forward in understanding universality out of equilibrium [150,151].

## ACKNOWLEDGMENTS

We thank E. Altman, M. Foster, A. Hemmerich, H. Kessler, A. Polkovnikov, A. M. Rey, M. Schleier-Smith, D. Stamper-Kurn, and M. Stefanini for stimulating discussions. This project has been supported by the Deutsche Forschungsgemeinschaft (DFG, German Research Foundation) through Project ID No. 429529648-TRR 306 QuCoLiMa (Quantum Cooperativity of Light and Matter), No. 422213477-TRR 288 (Project No. B09), and Grant No. HADEQUAM-MA7003/3-1; by the Dynamics and Topology Center, funded by the State of Rhineland Palatinate; and in part by the National Science Foundation under Grant No. NSF PHY-1748958 (KITP program Non-Equilibrium Universality: From Classical to Quantum and Back). We further acknowledge funding from the SNF (Project No. IZBRZ2 186312). The work of R.F. has been supported by the ERC under Grant Agreement No. 101053159 (RAVE). Parts of this research were conducted using the Mogon supercomputer and/or advisory services offered by Johannes Gutenberg University Mainz [152], which is a member of the AHRP (Alliance for High Performance Computing in Rhineland Palatinate [153], and the Gauss Alliance e.V.) We gratefully acknowledge the computing time granted on the Mogon supercomputer at Johannes Gutenberg University Mainz [154] through the project DysQCorr.

## APPENDIX A: COMPUTATION OF THE LYAPUNOV EXPONENT

Here we give further details about the calculation of the Lyapunov exponent referring specifically to the results in Sec. IV B. We extract the Lyapunov exponent investigating the divergence of  $R$  nearly sampled initial conditions. We use as measure of the distance of two trajectories the Frobenius norm of the difference of the average one-body reduced density matrices, namely,

$$\Delta\Sigma(i, j, t) = \sqrt{\sum_{n,m=1}^N |\Sigma_{n,m}(i, t) - \Sigma_{n,m}(j, t)|^2}, \quad (\text{A1})$$

where  $i, j \in [1, R]$  label the trajectory and  $t$  is the time. The  $R$  initial states are sampled such that  $\Delta\Sigma(i, j \neq i, t=0) \approx 10^{-8}$ . Then, we compute the average distance over all the trajectories

$$\Delta\Sigma(t) = \frac{2}{R(R-1)} \sum_{i=1}^R \sum_{j=i+1}^R \Delta\Sigma(i, j, t). \quad (\text{A2})$$

The dynamics is regular when  $\Delta\Sigma(t)$  grows polynomially in time, while it is chaotic if  $\Delta\Sigma(t)$  grows exponentially in time,

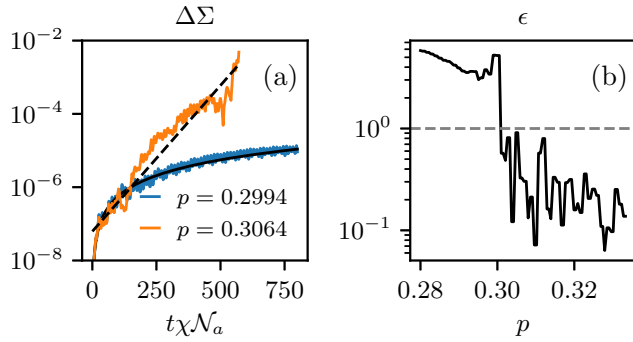


FIG. 9. (a) Dynamics of the average distance between  $R = 12$  nearly sampled trajectories starting from two multimode Schrödinger cat states parameterized by  $p$  [cf. Eq. (16)] in the  $N = 3$  level spin-exchange model. We fix two different values of  $p = \{0.2994, 0.3064\}$ . The continuous line is the polynomial fit. The dashed line is the exponential fit. (b) Relative error between the exponential fit and the polynomial fit. When  $\epsilon > 1$  ( $\epsilon < 1$ ), the polynomial (exponential) fit better approximates the data. The horizontal dashed gray line is at  $\epsilon = 1$ . Notice the sharp change of  $\epsilon$  around  $p \approx 0.3$ . The parameters of the simulations are the same as the one in Fig. 4 in the main text.

with the largest Lyapunov exponent equal to the rate of the exponential. In Fig. 9(a), we show two paradigmatic examples in the regular phase and chaotic phase. Specifically, referring to the results in Fig. 4, we fix  $p \lesssim p^*$  and  $p \gtrsim p^*$  with  $p^* \approx 0.3$  to highlight the abrupt change of the behavior of  $\Delta\Sigma(t)$ . In Fig. 9(b), we show the relative error  $\epsilon$  between the exponential fit and the polynomial fit. When  $\epsilon > 1$  ( $\epsilon < 1$ ), the polynomial (exponential) fit better approximates the data. We checked that our results are not affected by decreasing the time step.

#### APPENDIX B: CHAOS INDUCED UPON TRADING SU(2) WITH SU(3) INTERACTIONS IN THREE-LEVEL SYSTEM

Here, we investigate the onset of a chaotic phase in the three-level spin-exchange model starting from a separable state in Eq. (5) with  $|\psi_j\rangle$  in a Schrödinger cat state parameterized by  $p$  via Eq. (16). In Fig. 10, we show the maximum Lyapunov exponent as a function of the ratio  $g_1/g_2 = \tan(\theta)$  and  $p$  in the homogeneous case ( $W = 0$ ). For  $\theta/\pi = \{0, 0.25, 0.5\}$ , the Hamiltonian can be written in terms of a SU(2) subgroup of SU(3), and since dynamics are therefore restricted to that subgroup there is no chaos for any value of  $p$ . Furthermore, for  $\theta/\pi = \{0, 0.5\}$  we have  $g_1 = 0$  and  $g_2 = 0$ , respectively, thus we recover the SU(2) two-level system limit. As  $\theta/\pi$  deviates from the SU(2) limits, the system displays chaotic behavior for sufficiently large  $p$ . Deep in the SU(3) limit, we observe chaos for any  $p \gtrsim p^*$ , while near the SU(2) limit there are islands of chaotic behavior embedded in regular ones. We compute the Lyapunov exponent following the procedure described in Appendix A. Additionally, we manually set  $\sigma/(\chi\mathcal{N}) = 0$  when it is less than 0.01, since our procedure was signaling chaos in regions where, by direct inspection, there were no signatures of it.

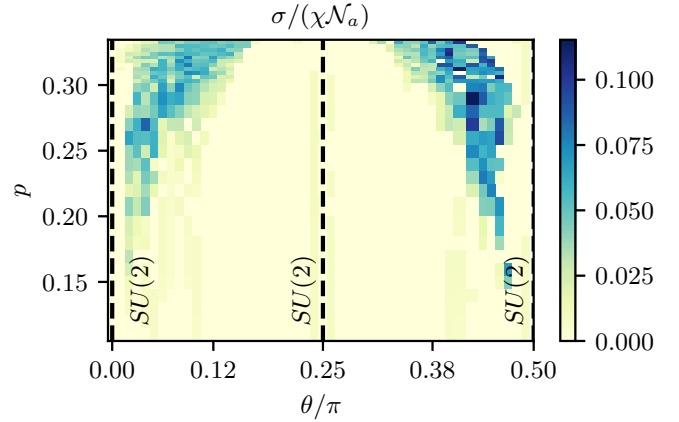


FIG. 10. Lyapunov exponent as a function of  $p$  and  $\theta$  in the  $N = 3$  spin-exchange model. The initial state is a multimode Schrödinger cat state parameterized by  $p$  via Eq. (16). We set  $\mathcal{N}_a \rightarrow \infty$  and  $W = 0$ . The vertical dashed lines are along the SU(2) limit, where the dynamics is effectively taking place in a SU(2) subgroup of SU(3). The all-to-all couplings are parameterized such that  $\chi_{1,1} < \chi_{2,2}$  for  $\theta/\pi \in [0, 0.25)$ ,  $\chi_{1,1} > \chi_{2,2}$  for  $\theta/\pi \in (0.25, 0.5]$ , and  $\chi_{1,1} = \chi_{2,2}$  at  $\theta/\pi = 0.25$ . In the SU(2) limits ( $\theta/\pi = \{0, 0.25, 0.5\}$ ), the dynamical response is regular for any value of  $p$ , since the couplings constrict the dynamics to take place in a SU(2) subspace of SU(3). Deep in the SU(3) limit ( $\theta/\pi \approx 0.1$  and  $\theta/\pi \approx 0.4$ ),  $|\Sigma_{n,m}|$  displays exponential sensitivity for any value of  $p \gtrsim p^*$ , with  $p^*$  dependent on  $\theta$ . Near the SU(2) two-level limits ( $\theta/\pi = \{0, 0.5\}$ ), we observe chaotic regions embedded in regular ones.

#### APPENDIX C: CHAOS INDUCED BY A FINITE FRACTION OF SCHRÖDINGER CAT STATES IN SU(3) SPIN-EXCHANGE HAMILTONIAN

Here, we provide additional details about the results discussed in Sec. IV C. We consider the Schrödinger cat state  $|\psi_{\text{cat}}\rangle \sim (|\tilde{\gamma}^{(1)}\rangle + |\tilde{\gamma}^{(2)}\rangle)$  defined in Eq. (16) and parameterized via  $p$ , while we consider  $|\tilde{\gamma}^{(1)}\rangle$  as coherent state. We initialize a fraction  $F$  of Schrödinger cat states  $|\psi_{\text{cat}}\rangle$ , such that the initial state is

$$|\Psi\rangle = \otimes_{j=1}^{\lfloor FL \rfloor} |\psi_{\text{cat}}\rangle \otimes_{j=\lfloor FL \rfloor + 1}^L |\tilde{\gamma}^{(1)}\rangle, \quad (\text{C1})$$

where  $\lfloor x \rfloor$  returns the least integer greater than or equal to  $x$ . The evolution is governed by the SU(3) spin-exchange Hamiltonian at  $W = 0$  and  $g_1/g_2 \approx 2$  (in units adopted in Fig. 10 it corresponds to  $\theta/\pi = 0.36$ ). In Fig. 11, we show the Lyapunov exponent as a function of  $p$  and  $F$ . For  $F < F^*$  the system displays regular dynamics, while for  $F > F^*$  the system enters in a chaotic regime. The Lyapunov exponent is computed following the same procedure discussed in Appendix A.

#### APPENDIX D: OPTIMIZATION PROCEDURE

Here we give further details about the practical implementation of steps (ii) and (iv) in the optimization procedure discussed in Sec. V. We set as initial guess for the initial state  $\tilde{\Sigma}_{n,m}(t=0) = \Sigma_{n,m}(t=\tau)$ , with the time  $\tau$  large enough, such that the initial transient dynamics is neglected. We set  $\tilde{h}_n = \sum_{j=1}^L h_j^{(n)}/L = 0$  and  $\tilde{\chi}_{n,m} = \chi_{n,m}$ , as initial guesses for

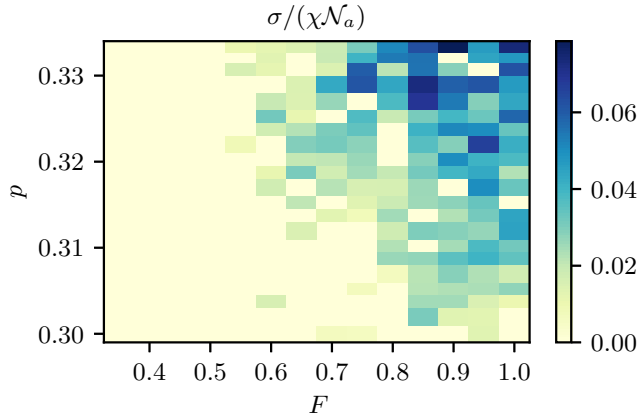


FIG. 11. Lyapunov exponent for the  $N = 3$  levels spin-exchange Hamiltonian in the homogeneous case ( $W = 0$ ) as a function of the initialized fraction  $F$  of multimode Schrödinger cat states in the state in Eq. (C1). The results were obtained simulating  $L = 100$  sites at fixed  $g_1/g_2 \approx 2$  (in the units adopted in Fig. 10 it corresponds to  $\theta/\pi = 0.36$ ). The results are not affected upon increasing  $L$ .

the parameters. Throughout the procedure, we keep  $\tilde{\zeta}_{n,m} = \tilde{v}_{n,m} = 0$  since they control processes absent in the bare model. Then, we numerically optimize both the initial state  $\{\tilde{\Sigma}_{n,m}(t=0)\}$  and the parameters  $\{\tilde{h}_n, \tilde{\chi}_{n,m}\}$  to minimize the cost function in Eq. (19) in the main text. The optimization procedure stops when the relative change between two consecutive iterations of the guessed solutions is less than  $\approx 10^{-2}$ .

We also test the convergence of the optimization procedure modifying the cost function. Specifically, we consider as cost function the average norm-2 distance

$$\epsilon_2 = \frac{1}{T} \int_0^T \sqrt{\sum_{n,m=1}^N |\tilde{\Sigma}_{n,m}(t) - \Sigma_{n,m}(t)|^2} dt, \quad (\text{D1})$$

and compare with the one based on the norm-1 cost function in Eq. (19). We test the two procedures using the same parameters and initial state of Fig. 5 in the main text, namely,  $W/(\chi \mathcal{N}_a) = 0.1$ ,  $g_2/g_1 \approx 10^{-2}$  and a permutationally invariant (in space) bosonic coherent state. Once the two procedures converged, we compare them computing the norm-1 distance between the optimized  $\tilde{\Sigma}(t)$  and  $\Sigma(t)$  obtained from the full many-body dynamics. We obtain  $\epsilon_1/\epsilon_2 \approx 0.6$  [where  $\epsilon_2$  is the norm-1 computed at the end of the optimization procedure based on the minimization of the norm-2 in Eq. (D1)] showing a slight advantage of norm-1 over the norm-2 in the optimization procedure.

## APPENDIX E: DYNAMICS WITH CAVITY LOSSES

The dynamics of the matter-light system can be described by the master equation for the density matrix:

$$\frac{d\hat{\rho}}{dt} = -i[\hat{H}, \hat{\rho}] + \mathcal{L}_c[\hat{\rho}] + \mathcal{L}_a[\hat{\rho}]. \quad (\text{E1})$$

Here,  $\hat{H}$  is the Hamiltonian in Eq. (1), where now the photon is an active DOF, and

$$\begin{aligned} \mathcal{L}_c[\hat{\rho}] &= \frac{\kappa}{2} (2\hat{a}\hat{\rho}\hat{a}^\dagger - \hat{a}^\dagger\hat{a}\hat{\rho} - \hat{\rho}\hat{a}^\dagger\hat{a}) \\ \mathcal{L}_a[\hat{\rho}] &= \frac{\eta}{2} \sum_{j=1}^L \sum_{n=1}^{N-1} (2\hat{\Sigma}_{n,n+1}^{(j)}\hat{\rho}\hat{\Sigma}_{n+1,n}^{(j)} - \hat{\Sigma}_{n+1,n}^{(j)}\hat{\Sigma}_{n,n+1}^{(j)}\hat{\rho} \\ &\quad - \hat{\rho}\hat{\Sigma}_{n+1,n}^{(j)}\hat{\Sigma}_{n,n+1}^{(j)}) \end{aligned} \quad (\text{E2})$$

are the Lindblad terms that describe the cavity-photon loss with decay rate  $\kappa$  and emission of single-atom excitation with rate  $\eta$ . From now on, we set  $\lambda_n = 0$  in the Hamiltonian  $\hat{H}$  and we consider the far detuned regime of the cavity mode as we are mainly interested in the spin-exchange interaction case. We perform adiabatic elimination such that [135–139]

$$\hat{a}(t) \approx - \sum_{n=1}^{N-1} \frac{ig_n \hat{\Sigma}_{n,n+1}(t)}{(i\omega_0 + \kappa/2)}. \quad (\text{E3})$$

In this regime the dynamics of the density matrix of the matter DOFs  $\hat{\rho}_m$  is given by the matter-only master equation:

$$\frac{d\hat{\rho}_m}{dt} = -i[\hat{H}_{\text{ad}}, \hat{\rho}_m] + \mathcal{L}_\Gamma[\hat{\rho}_m] + \mathcal{L}_a[\hat{\rho}_m]. \quad (\text{E4})$$

Here,  $\hat{H}_{\text{ad}}$  is the Hamiltonian given in Eq. (2), with  $v_{n,m} = \zeta_{n,m} = 0$  and all-to-all couplings per particle:

$$\chi_{n,m} = \frac{g_n g_m \omega_0}{\omega_0^2 + (\kappa/2)^2}. \quad (\text{E5})$$

The dissipative part  $\mathcal{L}_\Gamma[\hat{\rho}_m]$  is given by

$$\begin{aligned} \mathcal{L}_\Gamma[\hat{\rho}_m] &= \sum_{n,m=1}^{N-1} \frac{\sqrt{\Gamma_n \Gamma_m}}{2} (2\hat{\Sigma}_{n,n+1}\hat{\rho}_m\hat{\Sigma}_{m+1,m} \\ &\quad - \hat{\Sigma}_{n+1,n}\hat{\Sigma}_{m,m+1}\hat{\rho}_m - \hat{\rho}_m\hat{\Sigma}_{n+1,n}\hat{\Sigma}_{m,m+1}), \end{aligned} \quad (\text{E6})$$

where

$$\Gamma_n = \frac{g_n^2 \kappa}{\omega_0^2 + (\kappa/2)^2} \quad (\text{E7})$$

is the decay rate per particle of the collective DOFs. Imposing  $\mathcal{N}_a \chi_{n,m} \gg \mathcal{N}_a \sqrt{\Gamma_n \Gamma_m}$  and  $\mathcal{N}_a \chi_{n,m} \gg \eta$ , we obtain the conditions discussed in the main text.

- [1] K. Baumann, C. Guerlin, F. Brennecke, and T. Esslinger, Dicke quantum phase transition with a superfluid gas in an optical cavity, *Nature (London)* **464**, 1301 (2010).
- [2] H. Ritsch, P. Domokos, F. Brennecke, and T. Esslinger, Cold atoms in cavity-generated dynamical optical potentials, *Rev. Mod. Phys.* **85**, 553 (2013).
- [3] F. Mivehvar, F. Piazza, T. Donner, and H. Ritsch, Cavity qed with quantum gases: New paradigms in many-body physics, *Adv. Phys.* **70**, 1 (2021).

- [4] A. T. Black, H. W. Chan, and V. Vuletić, Observation of Collective Friction Forces due to Spatial Self-Organization of Atoms: From Rayleigh to Bragg Scattering, *Phys. Rev. Lett.* **91**, 203001 (2003).
- [5] H. Tanji-Suzuki, W. Chen, R. Landig, J. Simon, and V. Vuletić, Vacuum-induced transparency, *Science* **333**, 1266 (2011).
- [6] J. G. Bohnet, Z. Chen, J. M. Weiner, D. Meiser, M. J. Holland, and J. K. Thompson, A steady-state superradiant laser with less than one intracavity photon, *Nature (London)* **484**, 78 (2012).

- [7] F. Brennecke, R. Mottl, K. Baumann, R. Landig, T. Donner, and T. Esslinger, Real-time observation of fluctuations at the driven-dissipative Dicke phase transition, *Proc. Natl. Acad. Sci.* **110**, 11763 (2013).
- [8] J. Léonard, A. Morales, P. Zupancic, T. Donner, and T. Esslinger, Monitoring and manipulating Higgs and goldstone modes in a supersolid quantum gas, *Science* **358**, 1415 (2017).
- [9] M. Landini, N. Dogra, K. Kröger, L. Hruby, T. Donner, and T. Esslinger, Formation of a Spin Texture in a Quantum Gas Coupled to a Cavity, *Phys. Rev. Lett.* **120**, 223602 (2018).
- [10] R. M. Kroeze, Y. Guo, V. D. Vaidya, J. Keeling, and B. L. Lev, Spinor Self-Ordering of a Quantum Gas in a Cavity, *Phys. Rev. Lett.* **121**, 163601 (2018).
- [11] K. Baumann, R. Mottl, F. Brennecke, and T. Esslinger, Exploring Symmetry Breaking at the Dicke Quantum Phase Transition, *Phys. Rev. Lett.* **107**, 140402 (2011).
- [12] J. Klinder, H. Keßler, M. R. Bakhtiari, M. Thorwart, and A. Hemmerich, Observation of a Superradiant Mott Insulator in the Dicke-Hubbard Model, *Phys. Rev. Lett.* **115**, 230403 (2015).
- [13] V. D. Vaidya, Y. Guo, R. M. Kroeze, K. E. Ballantine, A. J. Kollár, J. Keeling, and B. L. Lev, Tunable-range, photon-mediated atomic interactions in multimode cavity QED, *Phys. Rev. X* **8**, 011002 (2018).
- [14] D. Nagy, J. K. Asbóth, P. Domokos, and H. Ritsch, Self-organization of a laser-driven cold gas in a ring cavity, *Europhys. Lett.* **74**, 254 (2006).
- [15] D. Nagy, G. Szirmai, and P. Domokos, Self-organization of a Bose-Einstein condensate in an optical cavity, *Eur. Phys. J. D* **48**, 127 (2008).
- [16] J. Klinder, H. Keßler, M. Wolke, L. Mathey, and A. Hemmerich, Dynamical phase transition in the open Dicke model, *Proc. Natl. Acad. Sci.* **112**, 3290 (2015).
- [17] M. R. Bakhtiari, A. Hemmerich, H. Ritsch, and M. Thorwart, Nonequilibrium Phase Transition of Interacting Bosons in an Intra-Cavity Optical Lattice, *Phys. Rev. Lett.* **114**, 123601 (2015).
- [18] M. A. Norcia, R. J. Lewis-Swan, J. R. K. Cline, B. Zhu, A. M. Rey, and J. K. Thompson, Cavity-mediated collective spin-exchange interactions in a strontium superradiant laser, *Science* **361**, 259 (2018).
- [19] J. A. Muniz, D. Barberena, R. J. Lewis-Swan, D. J. Young, J. R. Cline, A. M. Rey, and J. K. Thompson, Exploring dynamical phase transitions with cold atoms in an optical cavity, *Nature (London)* **580**, 602 (2020).
- [20] Z. Zhiqiang, C. H. Lee, R. Kumar, K. J. Arnold, S. J. Masson, A. S. Parkins, and M. D. Barrett, Nonequilibrium phase transition in a spin-1 Dicke model, *Optica* **4**, 424 (2017).
- [21] K. C. Cox, G. P. Greve, J. M. Weiner, and J. K. Thompson, Deterministic Squeezed States with Collective Measurements and Feedback, *Phys. Rev. Lett.* **116**, 093602 (2016).
- [22] R. J. Lewis-Swan, M. A. Norcia, J. R. K. Cline, J. K. Thompson, and A. M. Rey, Robust Spin Squeezing Via Photon-Mediated Interactions on an Optical Clock Transition, *Phys. Rev. Lett.* **121**, 070403 (2018).
- [23] I. D. Leroux, M. H. Schleier-Smith, and V. Vuletić, Implementation of Cavity Squeezing of a Collective Atomic Spin, *Phys. Rev. Lett.* **104**, 073602 (2010).
- [24] E. Pedrozo-Peñañiel, S. Colombo, C. Shu, A. F. Adiyatullin, Z. Li, E. Mendez, B. Braverman, A. Kawasaki, D. Akamatsu, Y. Xiao *et al.*, Entanglement on an optical atomic-clock transition, *Nature (London)* **588**, 414 (2020).
- [25] S. Colombo, E. Pedrozo-Peñañiel, A. F. Adiyatullin, Z. Li, E. Mendez, C. Shu, and V. Vuletić, Time-reversal-based quantum metrology with many-body entangled states, *Nat. Phys.* **18**, 925 (2022).
- [26] G. Barontini, L. Hohmann, F. Haas, J. Estève, and J. Reichel, Deterministic generation of multiparticle entanglement by quantum Zeno dynamics, *Science* **349**, 1317 (2015).
- [27] O. Hosten, R. Krishnakumar, N. J. Engelsen, and M. A. Kasevich, Quantum phase magnification, *Science* **352**, 1552 (2016).
- [28] H. Keßler, P. Kongkhambut, C. Georges, L. Mathey, J. G. Cosme, and A. Hemmerich, Observation of a Dissipative Time Crystal, *Phys. Rev. Lett.* **127**, 043602 (2021).
- [29] P. Kongkhambut, J. Skulte, L. Mathey, J. G. Cosme, A. Hemmerich, and H. Keßler, Observation of a continuous time crystal, *Science* **377**, 670 (2022).
- [30] N. Dogra, M. Landini, K. Kroeger, L. Hruby, T. Donner, and T. Esslinger, Dissipation-induced structural instability and chiral dynamics in a quantum gas, *Science* **366**, 1496 (2019).
- [31] D. Dreon, A. Baumgärtner, X. Li, S. Hertlein, T. Esslinger, and T. Donner, Self-oscillating pump in a topological dissipative atom-cavity system, *Nature (London)* **608**, 494 (2022).
- [32] Y. Guo, R. M. Kroeze, V. D. Vaidya, J. Keeling, and B. L. Lev, Sign-Changing Photon-Mediated Atom Interactions in Multimode Cavity Quantum Electrodynamics, *Phys. Rev. Lett.* **122**, 193601 (2019).
- [33] B. P. Marsh, Y. Guo, R. M. Kroeze, S. Gopalakrishnan, S. Ganguli, J. Keeling, and B. L. Lev, Enhancing Associative Memory Recall and Storage Capacity Using Confocal Cavity QED, *Phys. Rev. X* **11**, 021048 (2021).
- [34] P. Wolf, S. C. Schuster, D. Schmidt, S. Slama, and C. Zimmermann, Observation of Subradiant Atomic Momentum States with Bose-Einstein Condensates in a Recoil Resolving Optical Ring Resonator, *Phys. Rev. Lett.* **121**, 173602 (2018).
- [35] P. Kongkhambut, H. Keßler, J. Skulte, L. Mathey, J. G. Cosme, and A. Hemmerich, Realization of a Periodically Driven Open Three-Level Dicke Model, *Phys. Rev. Lett.* **127**, 253601 (2021).
- [36] Z. Zhang, C. H. Lee, R. Kumar, K. J. Arnold, S. J. Masson, A. L. Grimsmo, A. S. Parkins, and M. D. Barrett, Dicke-model simulation via cavity-assisted Raman transitions, *Phys. Rev. A* **97**, 043858 (2018).
- [37] E. J. Davis, G. Bentsen, L. Homeier, T. Li, and M. H. Schleier-Smith, Photon-Mediated Spin-Exchange Dynamics of Spin-1 Atoms, *Phys. Rev. Lett.* **122**, 010405 (2019).
- [38] F. Ferri, R. Rosa-Medina, F. Finger, N. Dogra, M. Soriente, O. Zilberberg, T. Donner, and T. Esslinger, Emerging Dissipative Phases in a Superradiant Quantum Gas with Tunable Decay, *Phys. Rev. X* **11**, 041046 (2021).
- [39] J. Marino, Y. Shchadilova, M. Schleier-Smith, and E. Demler, Spectrum, Landau-Zener theory and driven-dissipative dynamics of a staircase of photons, *New J. Phys.* **21**, 013009 (2019).
- [40] A. Periwal, E. S. Cooper, P. Kunkel, J. F. Wienand, E. J. Davis, and M. Schleier-Smith, Programmable interactions and emergent geometry in an array of atom clouds, *Nature (London)* **600**, 630 (2021).

- [41] K. Seetharam, A. Leroise, R. Fazio, and J. Marino, Dynamical scaling of correlations generated by short- and long-range dissipation, *Phys. Rev. B* **105**, 184305 (2022).
- [42] J. Marino, Universality class of Ising Critical States with long-range losses, *Phys. Rev. Lett.* **129**, 050603 (2022).
- [43] A. Piñeiro Orioli, J. K. Thompson, and A. M. Rey, Emergent Dark States from Superradiant Dynamics in Multilevel Atoms in a Cavity, *Phys. Rev. X* **12**, 011054 (2022).
- [44] R. Lin, R. Rosa-Medina, F. Ferri, F. Finger, K. Kroeger, T. Donner, T. Esslinger, and R. Chitra, Dissipation-Engineered Family of Nearly Dark States in Many-Body Cavity-Atom Systems, *Phys. Rev. Lett.* **128**, 153601 (2022).
- [45] M. Hayn, C. Emary, and T. Brandes, Phase transitions and dark-state physics in two-color superradiance, *Phys. Rev. A* **84**, 053856 (2011).
- [46] Y. Xu, D. Fallas Padilla, and H. Pu, Multicriticality and quantum fluctuation in a generalized Dicke model, *Phys. Rev. A* **104**, 043708 (2021).
- [47] J. Fan, G. Chen, and S. Jia, Atomic self-organization emerging from tunable quadrature coupling, *Phys. Rev. A* **101**, 063627 (2020).
- [48] J. Skulte, P. Kongkhambut, H. Keßler, A. Hemmerich, L. Mathey, and J. G. Cosme, Parametrically driven dissipative three-level Dicke model, *Phys. Rev. A* **104**, 063705 (2021).
- [49] J. G. Cosme, J. Skulte, and L. Mathey, Time crystals in a shaken atom-cavity system, *Phys. Rev. A* **100**, 053615 (2019).
- [50] E. J. Davis, A. Periwal, E. S. Cooper, G. Bentsen, S. J. Evered, K. Van Kirk, and M. H. Schleier-Smith, Protecting Spin Coherence in a Tunable Heisenberg Model, *Phys. Rev. Lett.* **125**, 060402 (2020).
- [51] M. A. Perlin, D. Barberena, M. Mamaev, B. Sundar, R. J. Lewis-Swan, and A. M. Rey, Engineering infinite-range  $SU(n)$  interactions with spin-orbit-coupled fermions in an optical lattice, *Phys. Rev. A* **105**, 023326 (2022).
- [52] D. Hemmer, E. Montañó, B. Q. Baragiola, L. M. Norris, E. Shojaei, I. H. Deutsch, and P. S. Jessen, Squeezing the angular momentum of an ensemble of complex multilevel atoms, *Phys. Rev. A* **104**, 023710 (2021).
- [53] L. M. Norris, C. M. Trail, P. S. Jessen, and I. H. Deutsch, Enhanced Squeezing of a Collective Spin Via Control of its Qudit Subsystems, *Phys. Rev. Lett.* **109**, 173603 (2012).
- [54] M. A. Norcia, J. R. K. Cline, J. A. Muniz, J. M. Robinson, R. B. Hutson, A. Goban, G. E. Marti, J. Ye, and J. K. Thompson, Frequency Measurements of Superradiance from the Strontium Clock Transition, *Phys. Rev. X* **8**, 021036 (2018).
- [55] P. Kirton and J. Keeling, Superradiant and lasing states in driven-dissipative Dicke models, *New J. Phys.* **20**, 015009 (2018).
- [56] E. A. Yuzbashyan, M. Dzero, V. Gurarie, and M. S. Foster, Quantum quench phase diagrams of an  $s$ -wave BCS-BEC condensate, *Phys. Rev. A* **91**, 033628 (2015).
- [57] J. Dukelsky, S. Pittel, and G. Sierra, Colloquium: Exactly solvable Richardson-Gaudin models for many-body quantum systems, *Rev. Mod. Phys.* **76**, 643 (2004).
- [58] R. W. Richardson, New class of solvable and integrable many-body models, [arXiv:cond-mat/0203512](https://arxiv.org/abs/cond-mat/0203512).
- [59] R. A. Barankov and L. S. Levitov, Synchronization in the BCS Pairing Dynamics as a Critical Phenomenon, *Phys. Rev. Lett.* **96**, 230403 (2006).
- [60] R. A. Barankov, L. S. Levitov, and B. Z. Spivak, Collective Rabi Oscillations and Solitons in a Time-Dependent BCS Pairing Problem, *Phys. Rev. Lett.* **93**, 160401 (2004).
- [61] M. Gaudin, Diagonalization of a class of spin hamiltonians, *J. Phys.* **37**, 1087 (1976).
- [62] R. Richardson and N. Sherman, Exact eigenstates of the pairing-force Hamiltonian, *Nucl. Phys.* **52**, 221 (1964).
- [63] E. A. Yuzbashyan, O. Tsypliyatsev, and B. L. Altshuler, Relaxation and Persistent Oscillations of the Order Parameter in Fermionic Condensates, *Phys. Rev. Lett.* **96**, 097005 (2006).
- [64] E. A. Yuzbashyan, B. L. Altshuler, V. B. Kuznetsov, and V. Z. Enolskii, Solution for the dynamics of the BCS and central spin problems, *J. Phys. A: Math. Gen.* **38**, 7831 (2005).
- [65] E. A. Yuzbashyan, B. L. Altshuler, V. B. Kuznetsov, and V. Z. Enolskii, Nonequilibrium cooper pairing in the nonadiabatic regime, *Phys. Rev. B* **72**, 220503(R) (2005).
- [66] S. P. Kelly, J. K. Thompson, A. M. Rey, and J. Marino, Resonant light enhances phase coherence in a cavity qed simulator of fermionic superfluidity, *Phys. Rev. Res.* **4**, L042032 (2022).
- [67] S. Smale, P. He, B. A. Olsen, K. G. Jackson, H. Sharum, S. Trotzky, J. Marino, A. M. Rey, and J. H. Thywissen, Observation of a transition between dynamical phases in a quantum degenerate Fermi gas, *Sci. Adv.* **5**, eaax1568 (2019).
- [68] F. Piazza and H. Ritsch, Self-ordered Limit Cycles, Chaos, and Phase Slippage with a Superfluid Inside an Optical Resonator, *Phys. Rev. Lett.* **115**, 163601 (2015).
- [69] B. Zhu, J. Marino, N. Y. Yao, M. D. Lukin, and E. A. Demler, Dicke time crystals in driven-dissipative quantum many-body systems, *New J. Phys.* **21**, 073028 (2019).
- [70] K. Tucker, B. Zhu, R. J. Lewis-Swan, J. Marino, F. Jimenez, J. G. Restrepo, and A. M. Rey, Shattered time: Can a dissipative time crystal survive many-body correlations? *New J. Phys.* **20**, 123003 (2018).
- [71] O. Chelpanova, A. Leroise, S. Zhang, I. Carusotto, Y. Tserkovnyak, and J. Marino, Competition between lasing and superradiance under spintronic pumping (2021), [arXiv:2112.04509](https://arxiv.org/abs/2112.04509).
- [72] A. Leroise, J. Marino, B. Žunkovič, A. Gambassi, and A. Silva, Chaotic Dynamical Ferromagnetic Phase Induced by Nonequilibrium Quantum Fluctuations, *Phys. Rev. Lett.* **120**, 130603 (2018).
- [73] S. B. Jäger, J. Cooper, M. J. Holland, and G. Morigi, Dynamical Phase Transitions to Optomechanical Superradiance, *Phys. Rev. Lett.* **123**, 053601 (2019).
- [74] S. B. Jäger, M. J. Holland, and G. Morigi, Superradiant optomechanical phases of cold atomic gases in optical resonators, *Phys. Rev. A* **101**, 023616 (2020).
- [75] E. I. Rodriguez Chiacchio and A. Nunnenkamp, Dissipation-Induced Instabilities of a Spinor Bose-Einstein Condensate Inside an Optical Cavity, *Phys. Rev. Lett.* **122**, 193605 (2019).
- [76] V. Ceban, P. Longo, and M. A. Macovei, Fast phonon dynamics of a nanomechanical oscillator due to cooperative effects, *Phys. Rev. A* **95**, 023806 (2017).
- [77] R. J. Lewis-Swan, D. Barberena, J. R. K. Cline, D. J. Young, J. K. Thompson, and A. M. Rey, Cavity-QED quantum Simulator of Dynamical Phases of a Bardeen-Cooper-Schrieffer Superconductor, *Phys. Rev. Lett.* **126**, 173601 (2021).
- [78] A. Shankar, E. A. Yuzbashyan, V. Gurarie, P. Zoller, J. J. Bollinger, and A. M. Rey, Simulating dynamical phases of

- chiral  $p + ip$  superconductors with a trapped ion magnet, *PRX Quantum* **3**, 040324 (2022).
- [79] E. Ibarra-García-Padilla, S. Dasgupta, H.-T. Wei, S. Taie, Y. Takahashi, R. T. Scalettar, and K. R. A. Hazzard, Universal thermodynamics of an  $SU(n)$  Fermi-Hubbard model, *Phys. Rev. A* **104**, 043316 (2021).
- [80] K. R. A. Hazzard, V. Gurarie, M. Hermele, and A. M. Rey, High-temperature properties of fermionic alkaline-earth-metal atoms in optical lattices, *Phys. Rev. A* **85**, 041604(R) (2012).
- [81] L. Bonnes, K. R. A. Hazzard, S. R. Manmana, A. M. Rey, and S. Wessel, Adiabatic Loading of One-Dimensional  $SU(n)$  Alkaline-Earth-Atom Fermions in Optical Lattices, *Phys. Rev. Lett.* **109**, 205305 (2012).
- [82] S.-K. Yip, B.-L. Huang, and J.-S. Kao, Theory of  $SU(n)$  Fermi liquids, *Phys. Rev. A* **89**, 043610 (2014).
- [83] M. Mamaev, T. Bilitewski, B. Sundar, and A. M. Rey, Resonant dynamics of strongly interacting  $SU(n)$  fermionic atoms in a synthetic flux ladder, *PRX Quantum* **3**, 030328 (2022).
- [84] A. Chu, A. P. Orioli, D. Barberena, J. K. Thompson, and A. M. Rey, Photon-mediated correlated hopping in a synthetic ladder, [arXiv:2208.01896](https://arxiv.org/abs/2208.01896) (2022).
- [85] L. Pezzè, A. Smerzi, M. K. Oberthaler, R. Schmied, and P. Treutlein, Quantum metrology with nonclassical states of atomic ensembles, *Rev. Mod. Phys.* **90**, 035005 (2018).
- [86] J. F. Rodríguez-Nieva, A. P. Orioli, and J. Marino, Universal prethermal dynamics and self-similar relaxation in the two-dimensional Heisenberg model, *PNAS* **119**(28), e2122599119 (2022).
- [87] M. Reitz, C. Sommer, and C. Genes, Langevin Approach to Quantum Optics with Molecules, *Phys. Rev. Lett.* **122**, 203602 (2019).
- [88] J. A. Campos-Gonzalez-Angulo, R. F. Ribeiro, and J. Yuen-Zhou, Generalization of the Tavis-Cummings model for multi-level anharmonic systems, *New J. Phys.* **23**, 063081 (2021).
- [89] C. Cohen-Tannoudji, J. Dupont-Roc, and G. Grynberg, *Atom-Photon Interactions* (Wiley, 1998).
- [90] P. Kirton and J. Keeling, Suppressing and Restoring the Dicke Superradiance Transition by Dephasing and Decay, *Phys. Rev. Lett.* **118**, 123602 (2017).
- [91] F. Brennecke, T. Donner, S. Ritter, T. Bourdel, M. Köhl, and T. Esslinger, Cavity QED with a Bose-Einstein condensate, *Nature (London)* **450**, 268 (2007).
- [92] A. Auerbach, *Interacting Electrons and Quantum Magnetism* (Springer Science & Business Media, New York, 2012).
- [93] H. Zhang and C. D. Batista, Classical spin dynamics based on  $SU(n)$  coherent states, *Phys. Rev. B* **104**, 104409 (2021).
- [94] K. Huang, *Introduction to Statistical Physics* (American Physical Society, 2009).
- [95] M. C. Gutzwiller, Effect of Correlation on the Ferromagnetism of Transition Metals, *Phys. Rev. Lett.* **10**, 159 (1963).
- [96] P. Kirton, M. M. Roses, J. Keeling, and E. G. Dalla Torre, Introduction to the Dicke model: From equilibrium to nonequilibrium, and vice versa, *Adv. Quantum Technol.* **2**, 1800043 (2019).
- [97] F. Carollo and I. Lesanovsky, Exactness of Mean-Field Equations for Open Dicke Models with an Application to Pattern Retrieval Dynamics, *Phys. Rev. Lett.* **126**, 230601 (2021).
- [98] E. Fiorelli, M. Müller, I. Lesanovsky, and F. Carollo, Mean-field dynamics of open quantum systems with collective operator-valued rates: validity and application, [arXiv:2302.04155](https://arxiv.org/abs/2302.04155).
- [99] B. Sciolla and G. Biroli, Dynamical transitions and quantum quenches in mean-field models, *J. Stat. Mech.: Theory Exp.* (2011) P11003.
- [100] P. Zapletal, A. Nunnenkamp, and M. Brunelli, Stabilization of multimode Schrödinger cat states via normal-mode dissipation engineering, *PRX Quantum* **3**, 010301 (2022).
- [101] L. Pezzè, M. Gessner, P. Feldmann, C. Klempt, L. Santos, and A. Smerzi, Heralded Generation of Macroscopic Superposition States in a Spinor Bose-Einstein Condensate, *Phys. Rev. Lett.* **123**, 260403 (2019).
- [102] B. C. Sanders, Entangled coherent states, *Phys. Rev. A* **45**, 6811 (1992).
- [103] B. C. Sanders, Review of entangled coherent states, *J. Phys. A: Math. Theor.* **45**, 244002 (2012).
- [104] V. Dodonov, Nonclassical states in quantum optics: A squeezed review of the first 75 years, *J. Opt. B: Quantum Semiclassical Opt.* **4**, R1 (2002).
- [105] J. A. Scaramazza, P. Smacchia, and E. A. Yuzbashyan, Consequences of integrability breaking in quench dynamics of pairing Hamiltonians, *Phys. Rev. B* **99**, 054520 (2019).
- [106] Y. Dong, L. Dong, M. Gong, and H. Pu, Dynamical phases in quenched spin-orbit-coupled degenerate Fermi gas, *Nat. Commun.* **6**, 6103 (2015).
- [107] A. Zabalo and E. A. Yuzbashyan, Time reversal symmetry protected chaotic fixed point in the quench dynamics of a topological  $p$ -wave superfluid, *Phys. Rev. B* **104**, 104505 (2021).
- [108] H. Goldstein, C. Poole, and J. Safko, *Classical Mechanics* (Pearson, 2002).
- [109] V. I. Arnold, *Mathematical Methods of Classical Mechanics* (Springer, New York, 1978).
- [110] O. Babelon, D. Bernard, and M. Talon, *Introduction to Classical Integrable Systems* (Cambridge University Press, 2003).
- [111] J. A. Campos-Gonzalez-Angulo and J. Yuen-Zhou, Generalization of the tavis-cummings model for multi-level anharmonic systems: Insights on the second excitation manifold, *J. Chem. Phys.* **156**, 194308 (2022).
- [112] N. M. Bogoliubov, R. K. Bullough, and J. Timonen, Exact solution of generalized Tavis-Cummings models in quantum optics, *J. Phys. A: Math. Gen.* **29**, 6305 (1996).
- [113] A. Glick, H. Lipkin, and N. Meshkov, Validity of many-body approximation methods for a solvable model: (III). Diagram summations, *Nucl. Phys.* **62**, 211 (1965).
- [114] C. Emary and T. Brandes, Chaos and the quantum phase transition in the Dicke model, *Phys. Rev. E* **67**, 066203 (2003).
- [115] M. A. Bastarrachea-Magnani, B. López-del-Carpio, S. Lerma-Hernández, and J. G. Hirsch, Chaos in the Dicke model: Quantum and semiclassical analysis, *Phys. Scr.* **90**, 068015 (2015).
- [116] J. Chávez-Carlos, B. López-del-Carpio, M. A. Bastarrachea-Magnani, P. Stránský, S. Lerma-Hernández, L. F. Santos, and J. G. Hirsch, Quantum and Classical Lyapunov Exponents in Atom-Field Interaction Systems, *Phys. Rev. Lett.* **122**, 024101 (2019).
- [117] S. Pilatowsky-Cameo, J. Chávez-Carlos, M. A. Bastarrachea-Magnani, P. Stránský, S. Lerma-Hernández, L. F. Santos, and J. G. Hirsch, Positive quantum Lyapunov exponents in experimental systems with a regular classical limit, *Phys. Rev. E* **101**, 010202(R) (2020).

- [118] J. Chávez-Carlos, M. A. Bastarrachea-Magnani, S. Lerma-Hernández, and J. G. Hirsch, Classical chaos in atom-field systems, *Phys. Rev. E* **94**, 022209 (2016).
- [119] Y. Alavirad and A. Lavasani, Scrambling in the Dicke model, *Phys. Rev. A* **99**, 043602 (2019).
- [120] M. A. Bastarrachea-Magnani, B. López-del-Carpio, E. J. Chávez-Carlos, S. Lerma-Hernández, and J. G. Hirsch, Delocalization and quantum chaos in atom-field systems, *Phys. Rev. E* **93**, 022215 (2016).
- [121] S. Lerma-Hernández, D. Villaseñor, M. Bastarrachea-Magnani, E. Torres-Herrera, L. F. Santos, and J. Hirsch, Dynamical signatures of quantum chaos and relaxation time scales in a spin-boson system, *Phys. Rev. E* **100**, 012218 (2019).
- [122] M. A. Bastarrachea-Magnani, B. L. del Carpio, J. Chávez-Carlos, S. Lerma-Hernández, and J. G. Hirsch, Regularity and chaos in cavity QED, *Phys. Scr.* **92**, 054003 (2017).
- [123] P. Barmettler, D. Fioretto, and V. Gritsev, Non-Equilibrium dynamics of gaudin models, *Europhys. Lett.* **104**, 10004 (2013).
- [124] R. Bonifacio and G. Preparata, Coherent spontaneous emission, *Phys. Rev. A* **2**, 336 (1970).
- [125] J. Keeling, Quantum corrections to the semiclassical collective dynamics in the Tavis-Cummings model, *Phys. Rev. A* **79**, 053825 (2009).
- [126] M. O. Scully and M. S. Zubairy, *Quantum Optics* (Cambridge University Press, 1999).
- [127] A. Das, K. Sengupta, D. Sen, and B. K. Chakrabarti, Infinite-range Ising ferromagnet in a time-dependent transverse magnetic field: Quench and ac dynamics near the quantum critical point, *Phys. Rev. B* **74**, 144423 (2006).
- [128] S. P. Kelly, E. Timmermans, and S.-W. Tsai, Detecting macroscopic indefiniteness of cat states in bosonic interferometers, *Phys. Rev. A* **100**, 032117 (2019).
- [129] S. P. Kelly, E. Timmermans, and S.-W. Tsai, Thermalization and its breakdown for a large nonlinear spin, *Phys. Rev. A* **102**, 052210 (2020).
- [130] N. Defenu, T. Enss, M. Kastner, and G. Morigi, Dynamical Critical Scaling of Long-Range Interacting Quantum Magnets, *Phys. Rev. Lett.* **121**, 240403 (2018).
- [131] A. E. Tarkhov, S. Wimberger, and B. V. Fine, Extracting Lyapunov exponents from the echo dynamics of Bose-Einstein condensates on a lattice, *Phys. Rev. A* **96**, 023624 (2017).
- [132] P. Gaspard, *Chaos, Scattering and Statistical Mechanics*, Cambridge Nonlinear Science Series, Vol. 9 (Cambridge University Press, England, 2005).
- [133] A. M. Rey, L. Jiang, M. Fleischhauer, E. Demler, and M. D. Lukin, Many-body protected entanglement generation in interacting spin systems, *Phys. Rev. A* **77**, 052305 (2008).
- [134] G. Bentsen, T. Hashizume, A. S. Buyskikh, E. J. Davis, A. J. Daley, S. S. Gubser, and M. Schleier-Smith, Treelike Interactions and Fast Scrambling with Cold Atoms, *Phys. Rev. Lett.* **123**, 130601 (2019).
- [135] *Quantum Optics*, edited by D. Walls and G. J. Milburn (Springer, Berlin, 2008).
- [136] S. B. Jäger, T. Schmit, G. Morigi, M. J. Holland, and R. Betzholtz, Lindblad Master Equations for Quantum Systems Coupled to Dissipative Bosonic Modes, *Phys. Rev. Lett.* **129**, 063601 (2022).
- [137] F. Damanet, A. J. Daley, and J. Keeling, Atom-only descriptions of the driven-dissipative Dicke model, *Phys. Rev. A* **99**, 033845 (2019).
- [138] M. Xu, S. B. Jäger, S. Schütz, J. Cooper, G. Morigi, and M. J. Holland, Supercooling of Atoms in an Optical Resonator, *Phys. Rev. Lett.* **116**, 153002 (2016).
- [139] S. B. Jäger, M. Xu, S. Schütz, M. J. Holland, and G. Morigi, Semiclassical theory of synchronization-assisted cooling, *Phys. Rev. A* **95**, 063852 (2017).
- [140] A. Chu, A. P. Orioli, D. Barberena, J. K. Thompson, and A. M. Rey, Photon-mediated correlated hopping in a synthetic ladder, [arXiv:2208.01896](https://arxiv.org/abs/2208.01896).
- [141] K. Seetharam, A. Leroose, R. Fazio, and J. Marino, Correlation engineering via nonlocal dissipation, *Phys. Rev. Res.* **4**, 013089 (2022).
- [142] S. P. Kelly, E. Timmermans, J. Marino, and S.-W. Tsai, Stroboscopic aliasing in long-range interacting quantum systems, *SciPost Phys. Core* **4**, 021 (2021).
- [143] R. Khasseh, A. Russomanno, and R. Fazio, Fragility of classical Hamiltonian period doubling to quantum fluctuations, *Phys. Rev. B* **104**, 134309 (2021).
- [144] G. Passarelli, P. Lucignano, R. Fazio, and A. Russomanno, Dissipative time crystals with long-range Lindbladians, *Phys. Rev. B* **106**, 224308 (2022).
- [145] G. Bentsen, I.-D. Potirniche, V. B. Bulchandani, T. Scaffidi, X. Cao, X.-L. Qi, M. Schleier-Smith, and E. Altman, Integrable and Chaotic Dynamics of Spins Coupled to an Optical Cavity, *Phys. Rev. X* **9**, 041011 (2019).
- [146] P. Strack and S. Sachdev, Dicke Quantum Spin Glass of Atoms and Photons, *Phys. Rev. Lett.* **107**, 277202 (2011).
- [147] S. Gopalakrishnan, B. L. Lev, and P. M. Goldbart, Frustration and Glassiness in Spin Models with Cavity-Mediated Interactions, *Phys. Rev. Lett.* **107**, 277201 (2011).
- [148] S. P. Kelly, R. Nandkishore, and J. Marino, Exploring many-body localization in quantum systems coupled to an environment via Wegner-Wilson flows, *Nucl. Phys. B* **951**, 114886 (2020).
- [149] M. Buchhold, P. Strack, S. Sachdev, and S. Diehl, Dicke-model quantum spin and photon glass in optical cavities: Nonequilibrium theory and experimental signatures, *Phys. Rev. A* **87**, 063622 (2013).
- [150] J. Marino, M. Eckstein, M. S. Foster, and A. M. Rey, Dynamical phase transitions in the collisionless pre-thermal states of isolated quantum systems: Theory and experiments, *Rep. Prog. Phys.* **85**, 116001 (2022).
- [151] W. Berdanier, J. Marino, and E. Altman, Universal Dynamics of Stochastically Driven Quantum Impurities, *Phys. Rev. Lett.* **123**, 230604 (2019).
- [152] [hpc.uni-mainz.de](https://hpc.uni-mainz.de).
- [153] [www.ahrp.info](http://www.ahrp.info).
- [154] [hpc.uni-mainz.de](https://hpc.uni-mainz.de).